Electron Transfer in Gas Surface Collisions

Electron Transfer in Gas Surface Collisions

academisch proefschrift

ter verkrijging van de graad van Doctor in de Wiskunde en Natuurwetenschappen aan de Universiteit van Amsterdam, op gezag van de Rector Magnificus, Dr. D.W. Bresters, hoogleraar in de Faculteit der Wiskunde en Natuurwetenschappen, in het openbaar te verdedigen in de Aula der Universiteit (tijdelijk Lutherse Kerk, ingang Singel 411, hoek Spui) op woensdag 19 januari 1983 des namiddags te 17.30 uur

door

Johannes Nicolaas Maria Van Wunnik

geboren te Valkenburg-Houthem

Promotor : Prof.Dr. J. Los

Co-referent: Prof.Dr. P.F. de Châtel

Aan mijn ouders

Contents

This thesis is based upon the following articles:

Chapter I : J.N.M. van Wunnik and J. Los:
Resonant Charge Transfer in Atom-Metal Surface Reactions.
Physica Scripta, to be published.

J.N.M. van Wunnik en P. Massmann:
Plasmafysische Toepassingen van Negatieve Ionen geproduceerd aan Oppervlakken.
Nederl.Tijdschrift v.Natuurkunde A48, 2 (1982).

Chapter II : B. Rasser, J.N.M. van Wunnik and J. Los:
Theoretical Models of the Negative Ionization of Hydrogen on Clean Tungsten, Cesiated Tungsten and Cesium Surfaces at Low Energies.
Surface Sci. 118, 697 (1982).

Chapter III : J.N.M. van Wunnik, J.J.C. Geerlings and J. Los:
The Velocity Dependence of the Negatively Charged Fraction of Hydrogen Scattered from Cesiated Tungsten.
Surface Sci., to be published.

Chapter IV : J.N.M. van Wunnik, R. Brako, K. Makoshi and D.M. Newns:
Effect of Parallel Velocity on Charge Fraction in Ion-Surface Scattering.
Surface Sci., accepted for publication.

Chapter V : J.N.M. van Wunnik, J.J.C. Geerlings, E.H.A. Granneman and J. Los:
The Scattering of Hydrogen from Cesiated Tungsten Surfaces.
Surface Sci., to be published.

J.N.M. van Wunnik, J.J.C. Geerlings and J. Los:
The Scattering of Molecular Hydrogen Ions from Cesiated Tungsten Surfaces.
Surface Sci., to be published.

J.N.M. van Wunnik, B. Rasser and J. Los:
H^- and D^- Formation by Scattering H^+ and D^+ from a Cesiated W(110) Surface.
Phys.Letters 6, 288 (1982).

The work described in this thesis is part of the research program of the Stichting voor Fundamenteel Onderzoek der Materie (Foundation for Fundamental Research on Matter) and was made possible by financial support from the Nederlandse Organisatie voor Zuiver-Wetenschappelijk Onderzoek (Netherlands Organization for the Advancement of Pure Research).

CHAPTER I

Introduction

1. GENERAL BACKGROUND

In recent years there has been a rising interest in the interaction of atoms with metal surfaces. Especially resonant electron transfer between atoms and metals has been the subject of many theoretical and experimental studies.

Some atoms like the alkalis, are easily ionized when they are on or near a metal surface. Adsorption of these atoms on a metal surface induces polar bonds between adsorbates and substrate, which results in a surface electrostatic dipole layer. With a coverage of half a monolayer this dipole layer can reduce the work function of the metal to 1/3 of the uncovered value.

Especially the pioneering work of Gadzuk [1] resulted in a theoretical description and calculation of this effect from first principles.

Since the days of Langmuir and Taylor [2] it also has been recognized that scattering of thermal alkali and alkaline earth-elements and many compounds of these elements on high work function metals is a very effective means to ionize these elements.

In addition, from incandescent low work function surfaces negative ions can be thermally emitted, especially the halide anions which have the highest electron affinities.

By making use of thermodynamical arguments, Saha and Langmuir [3,4] could describe the thermal emission of ions from metal surfaces. They derived an expression for the positive ionization coefficient β^+, which is defined as the positive ion fraction emitted from the surface,

$$\beta^+ = \frac{n^+}{n^+ + n^o} = \frac{1}{1 + \frac{g^o}{g^+} \exp(-\frac{\Phi - I}{kT})} \qquad (1)$$

where g^i is the statistical weight (degeneracy) of the relevant state, Φ the work function of the metal and I the ionization potential of the emitted atom. A similar relation can be derived for the emission of negative ions with an electron affinity S,

$$\beta^- = \frac{n^-}{n^- + n^o} = \frac{1}{1 + \frac{g^o}{g^-} \exp(-\frac{S - \Phi}{kT})} \qquad (2)$$

These relations are valid under (quasi-)equilibrium conditions. For thermal incident atomic beams the sticking factor commonly is close to unity, and the Saha-Langmuir equation can be applied with good results. For example for thermal emission of sodium from tungsten the Na^+ fraction is of the order of 40%, for thermal emission of hydrogen from a cesiated tungsten surface the H^- fraction is of the order of 0.01%.

Many experiments, however, indicate that much higher ionization efficiencies can be attained if the particles are emitted with higher (hyperthermal) velocities ($> 1.0 \cdot 10^4$ m/s). Evidence for this is obtained from Secondary Ion Mass Spectrometry, sputtering and in particular, from beam experiments in the eV range. This holds for positive as well as negative ionization.

Recently, the possibility of surface ionization - positive as well as negative ionization - by scattering hyperthermal ions or neutrals at a metal surface has been explored very intensively. This large interest is mainly due to the possibilities of applying surface ionization in input and output devices

of fusion experiments as for example neutral beam injectors and neutral particles detectors.

Neutral injection, that is the energy transfer of beams of high energetic neutral hydrogen or deuterium atoms to a hydrogen plasma, can be seen as one of the most promising methods for the heating of fusion plasmas. These high energetic neutral beams are made by first producing a low energetic positive or negative beam. These charged beams are accelerated to the required energies; hereafter neutralization of the fast ions takes place. Positive ion beam technology is at this moment the most advanced technique, but it becomes more and more clear that the required neutral beams of hundreds of keV and tens of amperes can be only efficiently produced by neutralization of H^- (D^-) ions (figure 1). One way to produce these negative hydrogen beams is by colliding protons with low work function surfaces like cesiated tungsten.

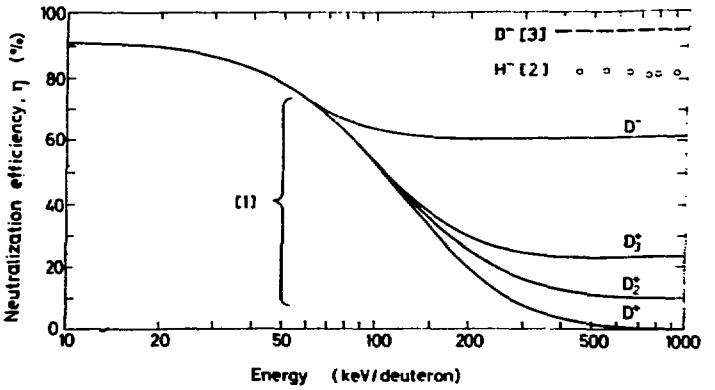

Fig. 1 - Neutralization efficiency for positive and negative ions. The efficiency for negative ions can be considerably increased by using for the neutralization a gas cel (1) instead of a plasma cel (2) or a laser-photodetachment cel (3).

Another field in which surface ionization is of practical use is the detection of low energetic (1 eV to 500 eV) hydrogen, alkali and alkaline earth atoms. By colliding the atoms

with a surface a part of the atoms will be negatively or positively charged, this depending on the surface work function and the affinity or ionization energy of the atom. After ionization acceleration and detection can take place.

This thesis deals with the fundamental aspects of negative ionization of hyperthermal hydrogen scattered on a cesiated tungsten surface. The velocity range is from $1.0 \cdot 10^4$ m/s (0.5 eV) to $6.5 \cdot 10^5$ m/s (2 keV).

In chapter II, the Gadzuk model, which describes the positive ionization of alkali atoms on a metal surface, is extended to the negative ionization of hydrogen on a metal surface. In the model used the motion of the particles is also incorporated. This is done in the framework of two existing methods; the probability method and the amplitude method. The results of both methods[*] are compared with each other.

In the probability as well as the amplitude method only the normal velocity is incorporated. However, in chapter III experimental evidence is given that also the parallel velocity of the particles is an important charge determining parameter. A mechanism to account for this parallel velocity dependence is proposed and treated in the probability method. In chapter IV this mechanism is treated within the amplitude method.

The hydrogen reflection process is of special interest for applications. In chapter V this process is studied for grazing incidence and cesiated surfaces. Grazing incidence is chosen because of the large reflection coefficients which are favourable for the applications.

2. THEORETICAL

2.1. Atom-metal interactions

Before discussing the ionization process of atoms scattered from a surface, at first the static situation of an atom at a given distance from a metal surface will be discussed.

When an atomic level is situated within the conduction band of a metal, resonant electron transitions between the metal and the atom will take place. The atomic level may be an

ionization level, which, when occupied, gives rise to a neutral atom, as well as an affinity level, which, when occupied, gives rise to a negative ion. Two different treatments are commonly used to describe such atom-metal interactions. Both treatments consider the interactions of the atoms with a semi-infinite metal substrate. The substrate, in both treatments, is represented by the uniform-background (jellium) model; in this model the ion core charge density is smeared out into a uniform positive charge density truncated stepwise at the surface.

In the first treatment the electron density distribution and the total energy are solved self-consistently in the Hartree-like local density functional (LDF) approximation. This LDF theory of many electron systems reduces the many-body problem for the ground state density distribution $n(\vec{r})$ of a system of N electrons in a static external potential $V(\vec{r})$ (due here to the atom nucleus and the positive background) to the self-consistent solution of a one-electron, Schrödinger-like equation. The effective potnetial in this equation is composed out of the external potential term $V(\vec{r})$, an exchange-correlation term and a term which accounts for the interaction of the electron considered with the other metal electrons [5,6]. The validity of this theoretical approach ranges from inside the bulk till about 3 a_o outside the surface.

In the second treatment the atom-metal interaction is considered as a perturbation of the pure atomic and metal states. This method was first proposed by Gurney [7] and later worked out by Gadzuk [1] for the chemisorption of alkalis on metal surfaces. This perturbational approach is valid for distances larger than 3 a_o. Both methods essentially lead to the same results. We will follow the second method, the perturbation approach, as this theory is better suited to describe the ionization probability of scattered particles. The theory will be simultaneously set up for positive as well as negative ionization. The formulae will be expressed in atomic units.

When a positive ion is close to a metal surface it will induce in the metal a negative image charge. This image charge will give rise to a shift of the ionization level which in

first approximation is given by the classical image potential formula:

$$\Delta E = \frac{1}{4Z} \tag{3}$$

Here Z is the ion surface distance. For a negative ion the shift of the affinity level will have the opposite sign (figure 2) and is given by

$$\Delta E = -\frac{1}{4Z} \tag{4}$$

These formulae are especially suited for large atom(ion)-surface distances (> 10 a_o), close to the surface deviations of this formula occur because of the finite screening length of the metal and the polarizability of the atom(ion). A good theoretical prediction of the positions of the ionization or affinity level for distances less than 10 a_o does not exist but those can be estimated by a trial and error method, see chapter II.

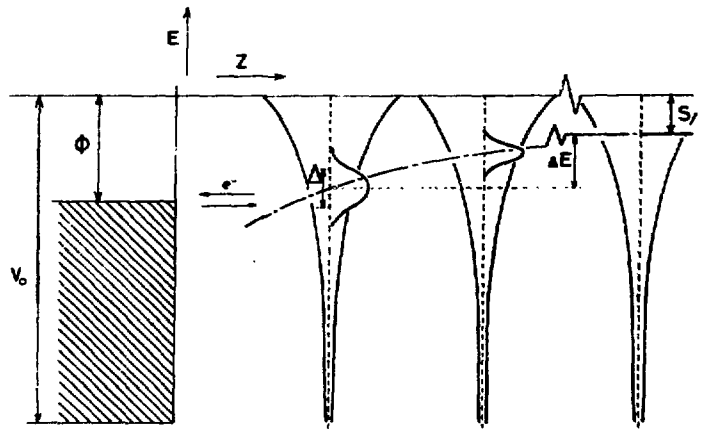

Fig. 2 - Potential energy diagram of the metal-adatom system. ϕ is the work function of the metal, the bottom of the conduction band is at $-V_o$, S is the affinity energy, Δ the level width and ΔE the shift of the affinity level. Δ and ΔE are given for three different adatom-metal distances.

If an atom is close to the surface the electronic wave functions of the atomic states and the metal states will overlap each other; this induces resonant transitions through the potential barrier between the metal and the atom.

In general the upwards shifted ionization level as well as the downwards shifted affinity level can both be populated with metal electrons. However, for the conversion to a negative ion the positive ion first has to be neutralized. So the transition probability of the electron between metal conduction band and affinity level of the atom is strongly dependent on whether the ionization level is populated or not. A model which simultaneously takes into account the interaction of the affinity level and the interaction of the ionization level with a metal is proposed by Rasser et al. [8]. In the following we will discuss the case where only one atomic level interacts with the metal. In case of the positive ionization of alkalis the one level assumption may be somewhat doubtful, due to the relatively small energy difference between ionization and affinity level. However, in the case of hydrogen, close to the surface, the separation between the ground state hydrogen level and the affinity level is still of the order of 10 eV which separation is so large that a neutral atom cannot be positively ionized. So if the hydrogen atom is in the neutral ground state the affinity level is the only level to be considered.

The transition matrix element between a metal state and an atomic state can be determined by rearrangement collision theory (ref. 1 and chapter II) and is given by

$$T_{\vec{k}i}(Z) = \langle \vec{k}|V|i\rangle \qquad (5)$$

in which Z is the atom-surface distance, $|\vec{k}\rangle$ is the metallic state, $|i\rangle$ the negative or neutral atomic electron state and V the unperturbed core potential of the neutral atom or positive ion outside the metal. In the case of positive ionization of the alkalis the positive ionic wave function is S shaped and the total electron spin is zero. So the interaction between the ion and the metal is in principle a three-body pro-

blem, namely between the alkali ion core, the metal and the electron in the metal $\vec{k}$ state that makes the transition (the active electron). The core potential V is given by $-1/r$, r being the distance between the active electron and ion core. For a neutral alkali or hydrogen atom the electron wave function is also shaped like an S wave, but the spin is 1/2. For the active electron there is thus an addition electron - electron interaction which changes the problem from a three-body problem into a four-body problem. The core potential V is here given by $-1/r_1 + 1/r_{12}$, where r_1 is the distance between active electron and proton and r_{12} is the distance between the electrons. For a detailed discussion of the calculation of the transition matrix element the reader is referred to [1] and ch. II.

The total transition rate is the sum of the transition rates of the individual metal states, where these states must be in resonance with the atom ionization or affinity level. So the total transition rate, given by the Fermi Golden rule is

$$\omega(Z) = 2\pi \sum_{\vec{k}} |T_{\vec{k}i}(Z)|^2 \delta(E_{\vec{k}} - E_a(Z)) = 2\pi \sum_{\text{deg}} \rho(E_a(Z)) |T_{\vec{k}i}(Z)|^2 \tag{6}$$

Here $E_a(Z)$ is the position of the level at the atom-surface distance Z, $\rho(E_a)$ is the density of states in the metal at E_a. The sum has to be taken over all the degeneracies of the metallic and ionic states. The metal wave functions and the density of states are determined in the framework of the free-electron model, $E_k = \frac{1}{2}|\vec{k}|^2$.

The transition rate gives rise to a finite lifetime of the state which means a Heisenberg broadening of the level. The width of the level is given by

$$\Delta(Z) = \omega(Z) \tag{7}$$

The metal states, which are in resonance with the level can be shown in first approximation to be a Lorentz distribution [8] about the metal states with $E_{\vec{k}} = E_a$. The half width of this distribution in $\vec{k}$ space is given by

$\sqrt{\Delta(Z)}/k_a$.

These resonance states are indicated by the shaded area in fig. 3a. The level width in first approximation is exponential decaying for increasing distance to the surface.

From the position of the affinity level and the level broadening, one now can determine the fraction of the particles $N^-(Z)$, $((N^+(Z))$ which are negatively (positively) charged at a given distance Z from the surface. In equilibrium $N^-(Z)$ is equal to that fraction of the total transition rate which is determined by filled metal states. $N^-(Z)$ can be obtained from:

$$N^-(Z) = \frac{\sum_{\vec{k}} |T_{\vec{k}i}(Z)|^2 \; L(E_{\vec{k}}, E_a(Z), \Delta(Z)) \; f(E_{\vec{k}}, E_F, T)}{\sum_{\vec{k}} |T_{\vec{k}i}(Z)|^2 \; L(E_{\vec{k}}, E_a(Z), \Delta(Z))} \qquad (8)$$

Here $L(E_{\vec{k}}, E_a(Z), \Delta(Z))$ is a Lorentz distribution with half width $\Delta(Z)$ around $E_a(Z)$, $f(E_{\vec{k}}, E_a, T)$ the Fermi distribution of the metal electrons with temperature T. The summation is taken over all metal states. For the positively charged fraction holds:

$$N^+(Z) = \frac{\sum_{\vec{k}} |T_{\vec{k}i}(Z)|^2 \; L(E_{\vec{k}}, E_a(Z), \Delta(Z)) \; (1 - f(E_{\vec{k}}, E_F, T))}{\sum_{\vec{k}} |T_{\vec{k}i}(Z)|^2 L(E_{\vec{k}}, E_a(Z), \Delta(Z))} \qquad (9)$$

The charge state of atoms at a given distance from the surface is according to (8) and (9) determined by the overlap between the broadened level and the metal conduction band. For an alkali atom close to the surface ($\lesssim 3\ a_o$) the level is above the conduction band and sc the particle will be positively charged. Far from the surface the charge state depends on the position of the ionization level with respect to the conduction band. If the ionization level is above the Fermi level the alkali atom will be positively charged, if the level is below the Fermi energy it will be neutral. For the affinity level holds that an overlap between affinity level and conduction

band gives rise to a negative ion. Increasing distance will give rise to a smaller overlap and so to a larger fraction of neutrals, see figure 2.

2.2. The motion of the atom (ion)

So far we only looked at the charge state of particles at a given distance from the surface. To determine the charge state of an atom after scattering we have to take into account the velocity of the particles. To incorporate the velocity in the theoretical description there are in principle two methods. One method is based on the time evolution of the probability of being in the state under consideration, the other method is based on the time evolution of the amplitude of the wave function amplitude for that state. In the following first the dependence on the normal component of the velocity will be discussed in terms of a qualitative method: the freezing method. Subsequently we will give a short description of the probability method and the amplitude method; normal as well as parallel components of the velocity will be considered. The discussion is focused on negative ionization.

2.2.1. The freezing method

The freezing method was first proposed by Overbosch et al. [9], to give a qualitative understanding of the positive ionization of sodium on tungsten.

An atom leaving a surface but being still close to it, is in strong interaction with that surface. The transition time of the active electrons is very small compared to the time the atom spends in front of the surface. Therefore in that region the atom leaves the metal adiabatically, at each distance the equilibrium charge fraction N^- will be established. On the other hand far from the surface there is almost no interaction between the atom and the metal. The charge state will not change at these distances. As a consequence at an intermediate distance, the so-called freezing distance, the charge state

will be frozen. The N^- value established at this distance will be maintained till infinite distance from the surface. For very low normal velocities the particle stays in equilibrium with the surface over a very large distance and so the freezing distance will be far out of the surface. With increasing normal velocity the adiabatic behaviour is broken up closer to the surface and so the freezing distance will shift to smaller values. So the behaviour of the final negative fraction with increasing normal velocity is thus determined by the behaviour of N^- for decreasing distances.

It can be shown that an H^- ion can only exist if the separation between ion and metal is at least of the order of the H^- radius [10]. Thus, close to the surface ($< 3\ a_o$) the negatively charged fraction drops despite the downwards shifted affinity level. For very large velocities ($> 5.0 \cdot 10^5$ m/s) the freezing distance comes in the region where the negative fraction drops and so the final H^- fraction will decrease. In other words: the neutral atom starting at the surface crosses the region in which the H^- ion can be formed so fast, that no metal electrons can populate the affinity level. The decrease of the negatively charged fraction will in first approximation be proportional to $1/v_\perp$.

2.2.2. *The probability method*

Before determining the fraction of negatively charged ions at an infinite distance from the surface, we first consider the evolution of the atom-metal system when the atom is at a given distance from the surface, but with an actual fraction of negatively ionized particles P_i which is not equal to the equilibrium fraction N^-. The time evolution of P_i can be described by the following equation:

$$\frac{dP_i(t)}{dt} = A(Z)\ [N^-(Z) - P_i(t)] \qquad (10)$$

For a moving particle we can transform this time dependent rate equation to a distance dependent equation by making use

of the time to distance relation of the particles with respect to the surface. For a straight line approximation of the trajectory and without taking the parallel velocity component into account we get

$$Z = Z_o + v_\perp t \tag{11}$$

where $v_\perp$ is the normal velocity component and Z_o the turning point of the trajectory. Eq. (10) can now easily be converted into

$$\frac{dP_i(Z)}{dZ} = \frac{\Delta(Z)}{v_\perp} \left[N^-(Z) - P_i(Z)\right] \tag{12}$$

The final fraction of negatively charged ions can be determined by integrating formula (12) from Z_o to infinity. The final negative charge fraction is then given by

$$\beta^-(v_\perp) = \frac{1}{v_\perp} \int_{Z_o}^{\infty} \Delta(Z)\, N^-(Z)\, \exp\left(-\frac{1}{v_\perp} \int_{Z}^{\infty} \Delta(Z')\, dZ'\right) dZ + \beta^-(Z_o)\, \exp\left(-\frac{1}{v_\perp} \int_{Z_o}^{\infty} \Delta(Z')\, dZ'\right) \tag{13}$$

Herein is $\beta^-(Z_o)$ the negative fraction at the turning point, which is assumed to be zero.

In the model described so far, no dependence on the parallel velocity is included. To do this we limit ourselves to situations where the atoms leave the surface under grazing angles. The velocity parallel to the surface is thus much larger than the velocity normal to the surface. Furthermore we limit ourselves to velocities where the screening of the ion by the metal electrons is still complete. The affinity level is then still at the same position as for the case that the parallel velocity is zero. This assumption is valid for most metals up till velocities of $7.0 \cdot 10^5$ m/s. On the other hand one can compare the maximum velocity of the metal electron with the parallel velocity of the atom. To make a transition to the atom, a single metal electron needs approximately the

same velocity parallel to the surface as the parallel velocity of the atom. At large parallel velocity there are less metal electrons able to make the transition than for small parallel velocity. So for particles moving parallel to the surface the negative fraction will be smaller than for particles with parallel velocity zero. The result is that on one hand the collective effect of the metal electrons is fast enough to screen the moving ion, but on the other hand the individual velocity of the electrons is not large enough to allow a transition.

For a more detailed picture we have to consider the way $N^-(Z)$ is determined. It does not matter whether the transition process is considered in the reference frame of the metal or the one of the atom. For simplicity we shall look at the problem from the point of view of the atom.

If the atom is fixed and the metal is moving with a velocity $\vec{v}_{||}$ at a given atom-metal distance Z, the metal electrons will get an additional velocity $\vec{v}_{||}$. The momentum of an electron with a momentum vector $\vec{k}$ in the metal frame then will become $\vec{k}+\vec{Q}$. Where $\vec{Q}$ is, in atomic units, equal to $\vec{v}_{||}$. In other words: the Fermi sphere will be shifted by $\vec{Q}$ in $\vec{k}$ space (see fig. 3b). The transition rate is unaffected by this shift because this rate is only determined by the number and position of states which are resonant with the affinity level and not by the fact whether these states are filled or not. The value of $N^-(Z)$, however, will change. $N^-(Z)$ again is determined by equation (8), but because the overlap between the states which are in resonance and the filled states is changed (see figure 3b) $N^-(Z)$ in most cases will be smaller than in the case $\vec{v}_{||}$ is zero. From equation (13) it is directly clear that a smaller $N^-(Z)$ value will result in a smaller final negative fraction at infinite distance from the surface. For a detailed description of the probability model and the incorporation of the parallel velocity in this model the reader is referred to chapter III.

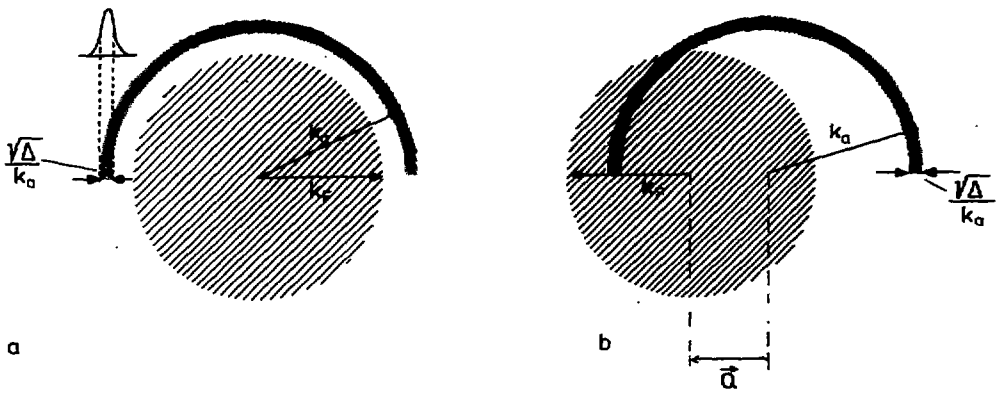

Fig. 3a - Schematic view of the metal $\vec{k}$ space. The shaded circle indicates the Fermi sphere. The dotted (half)ring indicates the metal states which are in resonance with the affinity level. Position and bandwidth of the affinity level correspond to respectively radius and width of the dotted ring. If the atom-metal distance decreases, the position of the affinity level shifts to lower energies and the width of the level becomes larger, the radius of the ring will decrease and the width of the ring will become larger. The overlap between the dotted ring and the circle determines N^-. In this scheme the parallel velocity is zero. $\frac{1}{2} k_F^2$ gives the position of the affinity level with respect to the bottom of the conduction band. $\frac{1}{2} k_F^2$ gives the position of the Fermi level.

Fig. 3b - In this scheme the parallel velocity is not zero. The overlap between the dotted ring and the shaded circle is changed with respect to figure 2a and so N^- will be different. $\vec{Q}$ is the additional momentum of the metal electrons seen from the moving atom.

2.2.3. The amplitude method

In this method we consider the time evolution of the atom-metal wave function during the scattering process. The parallel as well as the normal velocity component will be taken into account from the outset. In the probability method the parallel velocity is incorporated by looking to the atom-metal system as if the atom is fixed and the metal is moving. In this model we will use the reverse approach; namely a fixed metal and a moving atom. The Hamiltonian for a single electron of momentum $\vec{p} = (\vec{p}_{\parallel}, p_{\perp})$ and coordinate $\vec{x} = (\vec{x}_{\parallel}, z)$ is

$$H = \frac{\vec{p}^2}{2} + V(\vec{x}_{\parallel} - \vec{v}_{\parallel}t,\ z - Z(t)) + V_{eff}(z) \qquad (14)$$

where $\vec{v}_{\parallel}$ is the velocity parallel to the surface, $Z(t)$ the distance from atom to surface at time t, V is in the case of negative ionization the potential of the active electron in the neutral core potential and V_{eff} the effective potential of the jellium surface plus the perturbation potential induced by the dielectric response of the metal to the presence of both the neutral core and the active electron. The expansion of the total wave function in terms of pure metallic $\psi_{\vec{k}}(\vec{x})$ and atomic $\psi_a(\vec{x})$ wave functions, where the atomic and metallic states are assumed to be orthonormal, is

$$\psi = \sum_{\vec{k}} c_{\vec{k}}\psi_{\vec{k}}(\vec{x}) + c_a U\ \psi_a(\vec{x}_{\parallel},\ z - Z(t)) \qquad (15)$$

U is the Galilean transformation operator.

$$U = \exp(i\ \vec{v}_{\parallel} \cdot \vec{x}_{\parallel} - i\,t\,\vec{v}_{\parallel} \cdot \vec{p}_{\parallel}) \qquad (16)$$

and is such that $U\psi_a(\vec{x})\ \exp(-i\ E_a(Z)t)$ is a solution of the time-dependent Schrödinger equation for an atom at Z moving with uniform velocity $\vec{v}_{\parallel}$ parallel to the surface, with $E_a(Z)$ the energy eigenvalue of the orbital ψ_a at Z.

The expansion (15) is substituted into the time-dependent Schrödinger equation belonging to (14)

$$i\ \frac{\partial\psi}{\partial t} = H\psi \qquad (17)$$

when, multiplying by ψ_a or $\psi_{\vec{k}}$ and integrating over all $\vec{x}$, and using the assumed orthogonality of the a and $\vec{k}$ states, plus the algebra of the $\vec{p}_{||}$ and $\vec{x}_{||}$ operators in eq. (16), we obtain the Heisenberg equations of motion

$$i\,\dot{c}_a = E_a(t)c_a + \sum_{\vec{k}} c_{\vec{k}}\,\exp[i(E_{\vec{k}} - E_{\vec{k}-\vec{Q}})t]\;T_{(\vec{k}-\vec{Q})i}(t) \qquad (18)$$

$$i\,\dot{c}_{\vec{k}} = E_{\vec{k}}(t)c_{\vec{k}} + c_a\,\exp[-i(E_{\vec{k}} - E_{\vec{k}-\vec{Q}})t]\;T^{*}_{(\vec{k}-\vec{Q})i}(t) \qquad (19)$$

In eqs. (18,19) $E_{\vec{k}}$ is the energy eigenvalue $E_{\vec{k}} = \frac{1}{2}|k|^2$ of $\psi_{\vec{k}}$, $E_a(t) = E_a(Z(t))$, $\vec{Q} = \vec{v}_{||}$. The matrix element $T_{(\vec{k})i}(t)$ is given by

$$T_{(\vec{k})i}(t) = \langle\vec{k}|V(\vec{x}_{||}, z - Z(t))|i\rangle \qquad (20)$$

The expectation value of the charge state of the particle after scattering, i.e. the charge state at time $t\to\infty$ is given by

$$\langle n_a(\infty)\rangle = \langle c_a^{*}(\infty)\;c_a(\infty)\rangle \qquad (21)$$

By solving the equations (18) and (19) for c_a, substituting c_a into (21), making use of the wide band approximation [11] and by assuming a separability of the $\vec{k}$ and t dependence of $T_{(\vec{k})i}(t)$ into $P_{\vec{k}}u(t)$, we find

$$\langle n_a(\infty)\rangle = \sum_{|\vec{k}|} \Big|\int_{-\infty}^{\infty} \sqrt{\frac{\langle f(E_{\vec{k}+\vec{Q}},\,E_F,T)\,|P_{\vec{k}}|^2\rangle_\epsilon}{\langle|P_{\vec{k}}|^2\rangle_\epsilon}}\;\tfrac{1}{2}\Delta(t)$$

$$\times \exp\{-iE_{\vec{k}}t - \int_{t}^{\infty}[i\,E_a(t') + \tfrac{1}{2}\,\Delta(t')]\,dt'\}dt\Big|^2 \qquad (22)$$

where $f(E_{\vec{k}+\vec{Q}}, E_F, T)$ is the Fermi function

$$f(E_{\vec{k}+\vec{Q}}, E_F, T) = \frac{1}{\exp[\frac{\frac{1}{2}|\vec{k}+\vec{Q}|^2 - E_F}{kT}] + 1} \tag{23}$$

$\Delta(t)=\Delta(Z(t))$ is given by eq. (7) and $< >_\epsilon$ implies averaging over the surface $E_{\vec{k}} = \epsilon$.
For a motion parallel to the surface at a distance Z (22) can be converted into

$$<n_a(\infty)> = \int_{-V_o}^{\infty} d\epsilon \frac{<f(E_{\vec{k}+\vec{Q}}, E_F, T)\,|P_{\vec{k}}|^2>_\epsilon}{<|P_{\vec{k}}|^2>_\epsilon}$$

$$\times \frac{1}{\pi} \frac{\frac{1}{2}\Delta(Z)}{(\epsilon - E_a(Z))^2 + \frac{\Delta^2(Z)}{4}} \tag{24}$$

Here is $-V_o$ the position of the bottom of the conduction band with respect to the vacuum level. If on the scale of Δ the first part of the integrant is not strongly dependent on ϵ, the expression (24) is equal to the equilibrium charged fraction $N^-(Z)$ of eq. (8), in which the Fermi sphere is shifted over $\vec{Q}$. This result is the same as obtained for this situation with the probability method.

By assuming that also for particles leaving the surface the main contributions to $<n_a(\infty)>$ are coming from $\vec{k}$ states around $E_{\vec{k}} = E_a(Z)$ and that they are again on the scale of $\Delta(Z)$ not strongly dependent on ϵ, we can approximate (22) by

$$<n_a(\infty)> \approx \int_{-V_o}^{\infty} d\epsilon \left| \int_{-\infty}^{\infty} \sqrt{N^-(Z(t))\ \tfrac{1}{2}\Delta(t)} \right.$$

$$\left. \times \exp\{-i\epsilon\, t - \int_{t}^{\infty} [i\, E_a(t') + \tfrac{1}{2}\Delta(t')]dt'\}dt \right|^2 \tag{25}$$

In the case of negative hydrogen formation on low work function surfaces the final results of the amplitude and the probability method using the equations (13) and (25) respectively give within a few percent the same results (see chapter II). The main difference between both methods is seen for very low velocities ($< 1.0 \cdot 10^4$ m/s) where the charge state dependence on the velocity in the case of the probability method is linear while in the amplitude model this is proportional to $\exp(-1/v_\perp)$ [12]. The slower increase in the case of the amplitude model is due to destructive interference effects which give rise to a decrease of the ionization probability.

For a detailed discussion of the amplitude model is referred to chapter II and IV.

REFERENCES

[1] J.W. Gadzuk, Surface Sci. 6 (1967) 133.
[2] J. Taylor and I. Langmuir, Phys.Rev. 44 (1933) 423.
[3] M. Kaminsky, Atomic and Ionic Impact Phenomena on Metal Surfaces (Springer Verlag, Berlin 1965).
[4] E.Y. Zandberg and N.I. Ionov, Surface Ionization (IPST, Jeruzalem (1971).
[5] N.D. Lang and A.R. Williams, Phys.Rev.Lett. 34 (1975) 531.
[6] J.P. Muskat and D.M. Newns, Phys.Rev.B 19 (1979) 1270.
[7] R.W. Gurney, Phys.Rev. 47 (1935) 479.
[8] B. Rasser, M. Remy, Surface Sci. 93 (1980) 223.
[9] E.G. Overbosch, B. Rasser, A.D. Tenner and J. Los, Surface Sci. 92 (1980) 310.
[10] F.J. Rogers, H.C. Graboske and D.J. Harwood, Phys.Rev. A1 (1970) 1577.
[11] R. Brako and D.M. Newns, Surface Sic. 108 (1981) 253.
[12] B. Rasser, J.N.M. van Wunnik and J. Los, Surface Sci. 118 (1982) 697; this thesis chapter II.

CHAPTER II

Theoretical Models of Negative Ionization of Hydrogen on Cesiated Tungsten Surfaces

ABSTRACT

A theoretical study of the formation of negative hydrogen by colliding hydrogen (H^0,H^+) with a metal surface is presented.

The electron affinity level of an atom close to a metal surface is lowered due to the induction of image charges in the metal surface and is broadened due to resonant electron transitions between the conduction band of the metal and the valence shell of the atom. The position of the affinity level is determined by the combination of a calculation from first principles and a trial and error method, the level width is calculated from first principles.

The motion of the nucleus is incorporated by means of two methods: a probability method and an amplitude method. In both methods the electron motion is described quantum mechanically and the nuclear motion classically. In the probability model the time evolution of the ionization probability is considered, in the amplitude model the time evolution of the corresponding wave function amplitude is considered. In both methods only the normal velocity of the nucleus is incorporated.

The calculations give rise to maximum negative ionization efficiencies of 4% on W(110), 40% on cesiated tungsten and 15% on cesium.

1. INTRODUCTION

High power negative hydrogen (deuterium) ion beams are of very large interest for heating fusion plasmas because of the high neutralization efficiency above 100 keV energies [1]. The studies of Wiesemann et al. [2] have shown the importance of surface processes in the formation of H^- ions in a hollow cathode duoplasmatron. The idea of producing H^- (D^-) ion beams by a pure surface process has developed and is now a very promising one. This can be concluded from recent experimental studies [3] which report negative ionization efficiencies as high as 13% on cesium and 7% on thorium oxyge [4] and 40% on cesiated tungsten (110) [5]. However, for a better understanding of the experimental features and for optimizing a high power negative hydrogen ion source, a better theoretical knowledge of the surface process leading to the formation of negative ions is required

Although the interaction between neutral atoms (or positive ions) with a surface has been widely studied within the framework of chemisorption or of sputtering and secondary ion mass spectrometry (SIMS), interaction of negative ions with a surface is a newly opened field. One of the best models for describing particle-surface interaction is very likely the atom-jellium surface model [6]. This accurate model, however, does not include the dynamics of the particles. Velocity including time-dependent models separate the problem into two different motions: the motion of the centre of mass, described by classical mechanics, and the motion of the electrons. When the atom (or ion) approaches the surface, a resonant electron transition occurs between the valence shell of the hydrogen atom and the conduction band of the metal. In earlier theoretical studies [7,8] a model has been proposed where formation and decay of the negative ion are separated. In this model the formation of H^- is possible when the shifted affinity level is below the Fermi level. Survival of H^- in the outgoing trajectory is assumed to be exponentially dependent on the velocity. However, this arbitrary separation neither does take into account the metallic nature of the substrate [8,9], nor

the effect of the broadening of the adsorbate level, due to the finite lifetime of this level resulting from the transition of the active electron. The broadened level being partly filled [10], repetitive ionization and neutralization of the particle leaving the surface occurs, and this may invalidate the arbitrary separation of the process in an ionization and neutralization range, especially in the case of not too low work function substrates (as it was already mentioned by Hiskes [7]).

The purpose of this paper is to eliminate these approximations and to derive a more complete theory of the electron transfer between the atom (or ion) and the metal substrate. A quasi-adiabatic theory involving a time-dependent atom-surface interaction has already been shown to be quite adequate to describe the features of positive surface ionization of hyperthermal sodium atoms on a tungsten surface [11]. In this theory the time evolution of the ionization probability was calculated. Calculations based on this theory will be considered in section 3. Recently a time dependent amplitude theory has been developed [12]. This will be considered in section 4. The level shift and transition probabilities will be considered in section 2. The formulae will be expressed in atomic units.

2. LEVEL SHIFT AND LEVEL BROADENING

The discussion will be focused on the reflection of neutral hydrogen. Incident protons are not expected to give large deviations from the neutral hydrogen results. In front of a metal a proton ($v_\perp < 0.1$ a.u.) will have a large Auger neutralization probability [13]. This can be direct Auger neutralization in the ground state, or, more probable, first resonant neutralization in an excited state ($\approx 10\ a_o$ from the surface) followed by Auger de-excitation at small distances ($\approx 2\ a_o$). During the reflection at the surface and in the outgoing path the neutral atom can pick up an additional electron via a resonant process. The resonance is characterized by a level

position and a level width (fig. 1), which both will be discussed in this section.

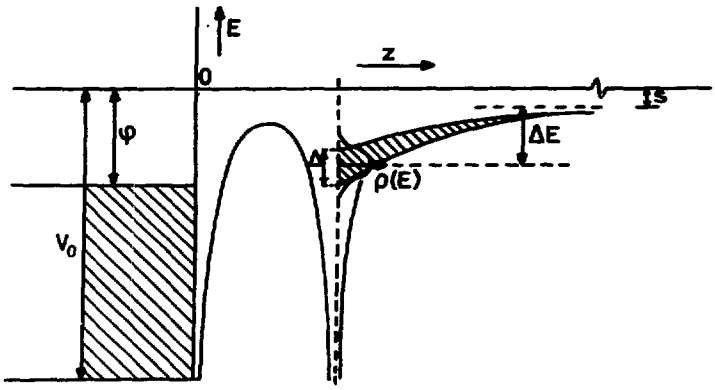

Fig. 1 - Energy level diagram for the interaction between a negative ion and a metallic surface.

Level shift

The behaviour of the position of the affinity level as a function of the atom-surface distance is chosen in accordance to the suggestions of Norskov et al. [14]. In this study the position of the affinity level was needed to calculate the chemiluminescence spectra observed during halogen chemisorption on sodium. The position in these calculations was in good agreement with the experimental results. The basic mechanism of the affinity level shift in front of a metal surface is the induction of a positive image charge in the metal surface. This positive image charge will give rise to a lowering of the affinity level. In principle the space can be divided into three regions:

- Far from the surface ($> 10\ a_o$); here the H^- ion is just slightly disturbed by the metal and so the decrease of the affinity level is given by the image potential formula [15]

$$\Delta E = \frac{1}{4(z + k_s^{-1})}$$

where z is the distance to the surface and k_s^{-1} the Debye screening radius.

- Close to the surface ($\lesssim 4\ a_o$); here the perturbation of the negative ion by the metal is strong, so the image potential formula is not applicable any more. Lang and Williams [6], however, showed that in this region the change of the affinity level is approximately given by the change of the effective potential (the local bottom of the conduction band). For cesium (Wigner-Leitz radius $r_s = 5.62$) the effective potential is determined by interpolating the self-consistently calculated effective potential values for $r_s = 5$ and $r_s = 6$ of Lang and Kohn [16]. For clean tungsten (110) and cesiated tungsten surfaces no effective potential values are available and therefore a somewhat different approach is used. The electron density of cesiated tungsten surfaces is given in an analytical form by Wojciechowski [17].

$$n(z, z_o, \theta) = 0.462\ n_W \exp(-1.23\ z) + \theta n_{Cs} \exp\left[-\frac{2.8}{\theta^2}\left(\frac{z - z_o}{z_o}\right)^2\right] \quad \text{for } z < z_o$$

$$= 0.462\ n_W \exp(-1.23\ z) + \theta n_{Cs} \exp\left[-\frac{0.693}{\theta^2}\left(\frac{z - z_o}{z_o}\right)^2\right] \quad \text{for } z > z_o$$

The degree of cesium surface coverage θ, the cesium atom-tungsten surface distance z_o and the free-electron densities of tungsten $n_{W(110)}$ and cesium n_{Cs} are the parameters in this formula.

Using these analytical forms, the effective potential acting on a metal electron as well as the work function of the surface can be calculated [17]. The cesium free-electron density n_{Cs} is equal to $1.33\ \ 10^{-3}\ a_o^{-3}$ [17]. $n_{W(110)}$ and z_o are chosen such that the work function of clean tungsten and cesiated tungsten ($\theta = 0.5$), calculated by using the expressions for $n(z, z_o, \theta)$ given above equals the experimental va-

lues 5.3 eV and 1.45 eV respectively. This procedure leads to a tungsten electron density of 73 10^{-3} a_o^{-3} and to a distance cesium-tungsten of 3.16 a_o. With these data of n_{Cs}, $n_{W(110)}$ and z_o the effective potential can be calculated as function of the surface distance and cesium coverage. The position of the affinity level is given by the effective potential minus the affinity energy.

- For intermediate distance (4 - 10 a_o) there exists some uncertainty about the level position. In this region neither the effective potential nor the image force approximation is valid. Therefore a function has to be chosen which connects the calculated effective potential ($z < 4$ a_o) with the image potential ($z > 10$ a_o). There is chosen for a straight line connection which starts at a certain point of the effective potential curve and which is tangent at the curve of the image potential at about 10 a_o.

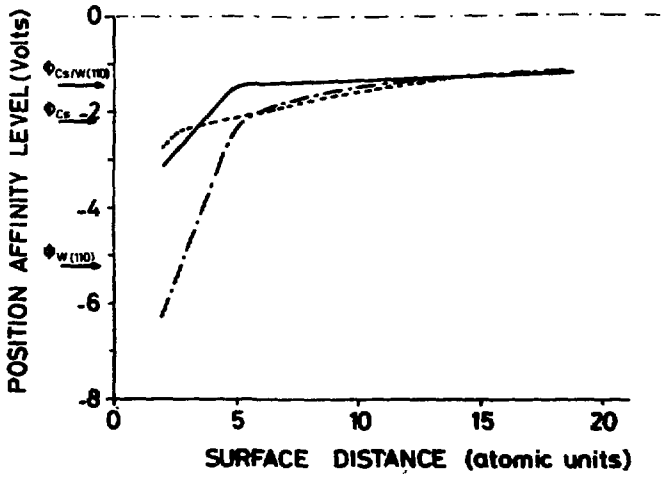

Fig. 2 - The position of the affinity level as a function of the distance to the surface. Three surfaces are used in the calculations, cesiated tungsten ———, cesium ----- and tungsten -.-.- .

The precise start position of the straight line is determined by a trial and error method. A certain start position will give in the $H^{o}(H^{+}) - H^{-}$ conversion probability calculations rise to a certain conversion probability. By changing the start position this probability can be made equal to the measured conversion probabilities. The measured conversion probabilities of 40% [5] on cesiated tungsten and 15% [13,18] on cesium give rise to a start position at resp. 4.75 a_o and 2.56 a_o. For a tungsten (110) target the effective potential and the image potential join more or less smoothly (fig. 2).

Level broadening

The lowered affinity level will activate the electron tunnelling process between the metal conduction band and the affinity level. This tunnelling process will give rise to a finite lifetime and thus to a broadening of the level.

Because the neutralization of the incident protons is complete and the position of the ionization level of the hydrogen atom with respect to the Fermi level of the substrate prevents resonant positive ionization of the hydrogen atom, the H^{-} formation process can be considered as a one-electron problem. It just involves a transition of a single electron (e_1 in fig. 3) and the only relevant terms of the total Hamiltonian of the

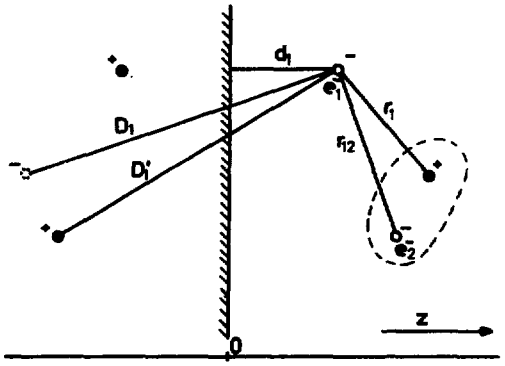

Fig. 3 - Electric image model for the interaction between a negative ion and a metallic surface.

system are those which are explicit functions of the coordinate of this electron (for a discussion of the other terms, see Gadzuk [19]), i.e.

$$H_1 = \tfrac{1}{2}\,\Delta_1 - \frac{1}{r_1} + \frac{1}{r_{12}} - \frac{1}{4d_1} + \frac{1}{D_1} - \frac{1}{D_1'} + V_{eff}(z_1) \qquad (1)$$

Here Δ_1 is the kinetic energy term of the active electron and $V_{eff}(z_1)$ is the effective potential of the jellium surface. As in the case of neutral atom-surface interaction [19], this Hamiltonian can be separated in two different ways and then be treated within a rearrangement collision theory. The active electron makes transitions between metallic and negative ion virtual states. The transition matrix element is given by [19]:

$$T_{if} = \langle \psi_m | V | \psi_i \rangle \qquad (2)$$

where ψ_m is the metallic wave function, ψ_i the negative ion wave function and V is the unperturbed core potential of the neutral atom acting on the active electron.

$$V = -\frac{1}{r_1} + \frac{1}{r_{12}}$$

Owing to the r_{12} term, the transition matrix element depends on the position of the electron e_2 (in fig. 3). This two-electron problem can be reduced to a one-electron problem by approximating the potential by a central potential and using for ψ_i a one-electron wave function $\psi_i(\vec{r}_1)$. The transition matrix element is then independent on the position of the electron e_2 and is given by:

$$T_{if} = \langle \psi_m(\vec{r}_1) | V(r_1) | \psi_i(\vec{r}_1) \rangle \qquad (3)$$

The central potential $V(r_1)$ is derived from the radial part $\phi(r_1)$ of the one-electron wave function ψ by:

$$V(r_1) = \frac{-1}{r_1} + \frac{1}{r_1}\int_0^{r_1} \phi^2(r_2)\, r_2^2\, dr_2 + \int_{r_1}^{\infty} \phi^2(r_2)\, r_2 dr_2 \qquad (4)$$

One-electron wave functions (e.g. Hartree-Fock wave functions) describe the negative hydrogen ion with respect to the configuration energy rather poorly. They even do not give a bound state of the ion. In the transition matrix element an asymptotic overlap of wave functions is involved and thus for our purpose a good spatial electron density distribution is much more important that an accurate configuration energy. Therefore a simple one-electron wave function is derived (see appendix) which gives a density distribution in agreement with more accurate correlated wave functions.

From this wave function we calculate the perturbing potential (4) and, by using for the metallic electron a free-electron like wave function [19], we obtain the transition matrix element (2). The transition rate is then given by:

$$\omega = 2\pi \sum_{\text{deg}} |T_{if}|^2 \rho_m(E) \qquad (5)$$

where $\rho_m(E)$ is the electron density of states within the metal and the sum has to be taken over all the degeneracies of the metallic and ionic states. The free-electron model is applied by which the depth of the conduction band is determined by summing the workfunction ϕ and the Fermi energy E_F. The width of the broadened level is derived from the transition rate by the Heisenberg relation.

The calculated electron transition rate $\omega(s^{-1})$ between an H^- ion, and tungsten, cesium and a cesiated tungsten surface are given in fig. 4 The corresponding level broadening $\Delta = \omega$ (eV) is indicated on the right-hand axis. They show that at large distances from the surface the transition probability decreases with increasing surface potential barrier V_o, owing to the decrease of the metallic wave function amplitude. The transition rate is an order of magnitude smaller than in the case of resonant positive ionization [11], this in spite of the sharper decay of the neutral atom wave function with respect to the negative ion wave function. The reason of this fact is that the shape of the negative ion potential is much sharper decreasing than the Coulomb potential felt by an electron in a neutral atom.

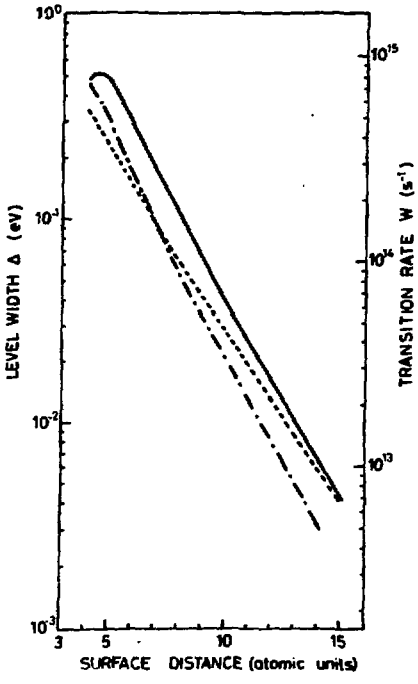

Fig. 4 - The level width as a function of the distance to the surface for cesiated tungsten ——, cesium ---- and tungsten -.-.- .

3 THE PROBABILITY MODEL

Till now the position of the affinity level and the transition rate of the active electron has been described, but no motion of the atom core has been taken into account. Before doing this, the charge state of a stationary hydrogen atom is considered. The negative charged fraction N^- according to Rasser and Remy [10] is given by the overlap between the broadened affinity level and the metal conduction band. The shape of the broadened affinity level can be shown to be Lorentzian [10] with a FWHM Δ.

$$N^- = \frac{1}{\pi} \int_{-V_o}^{-\phi} \frac{\Delta/2}{(\epsilon + S + \Delta E)^2 + \Delta^2/4} \cdot d\epsilon \qquad (6)$$

The temperature of the surface is taken to be zero, ϕ is the workfunction, S the affinity energy and ΔE the level shift. For the metal the free electron model is used. The position of the bottom of the conduction band is given by $-V_o$ with respect to the vacuum level.

The rate equation: When at a fixed distance from the surface the charge state is P_i, which is different from the equilibrium charge state N^-, the time evolution of the system is in first approximation described by:

$$\frac{dP_i(t)}{dt} = \Delta(z)\ [N^-(z) - P_i(t)] \qquad (7)$$

where the inverse transition rate $\omega^{-1}(z)$ $(= \Delta^{-1}(z))$ of the active electron will determine the time constant of the evolution process. For $t \to \infty$ the actual charge state $P_i(t)$ will converge to the equilibrium charge state $N^-(z)$. The time evolution of P_i of a moving atom can now be described by combining equation (7) and the time to surface distance relation of the moving atom. Making use of the straight line approximation,

$$z = z_o + v_z \cdot t$$

where only the outgoing trajectory is taken into account, z_o is the turning point of the trajectory and v_z the normal velocity component, the solution of equation (7) at $t \to \infty$ is given in atomic units by [11]

$$\beta^-(v_z) = P_i(\infty) = \frac{1}{v_z}\int_{z_o}^{\infty} \Delta(z)\ N^-(z)\ e^{-\frac{1}{v_z}\int_z^{\infty}\Delta(z')dz'}\,dz + P_i(o)\ e^{-\frac{1}{v_z}\int_{z_o}^{\infty}\Delta(z')dz'} \qquad (8)$$

The first part of this equation describes the formation of negatively charged particles along the outgoing trajectory, the second part describes the decay of the negative particles

which were already present at the turning point $P_i(o)$. Because of the relative long time the particles spend at the turning point, $P_i(o)$ is assumed to be equal to the equilibrium charge state at that point ($N^-(z_o)$). The results of the numerical solution of equation (8) for proton scattering on W(110), cesiated W(110) and cesium are shown in figs. 5, 6, 7.

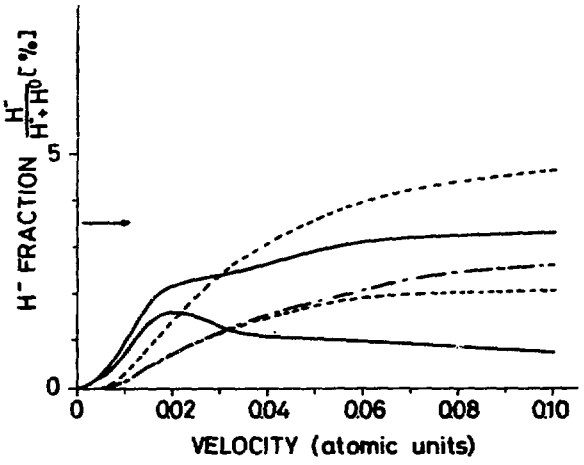

Fig. 5 - The H^- fraction of hydrogen scattered from a tungsten (110) surface as a function of the normal velocity component of the scattered particles. The charge state of a stationary atom at the turning point ($z_o = R_{W^{6+}} + R_{H^-} \approx 3\ a_o$) is indicated by the arrow. The exponential decay of this H^- charge fraction as function of the normal velocity component, which is equal in the amplitude model and the probability model, is indicated by -.-.- . The formation of H^- in the outgoing trajectory is for the probability model given by ——— and for the amplitude model by ----- . The total H^- fraction which is the sum of the exponential decay term and the formation term is for the probability model indicated by ——— and for the amplitude model by ----- .

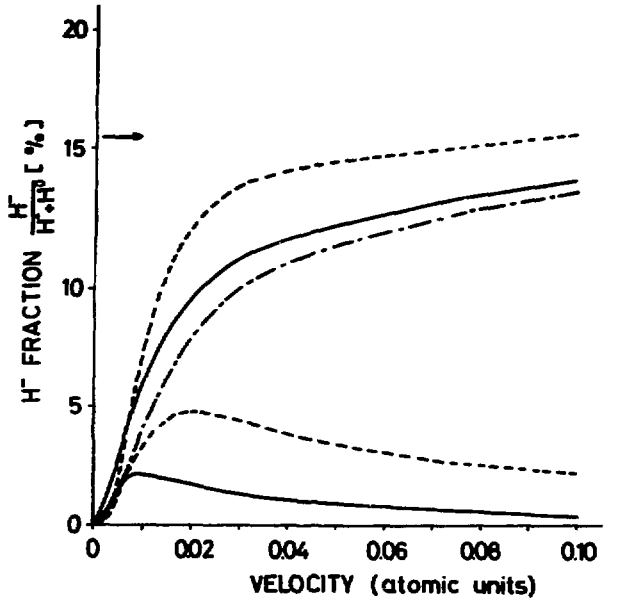

Fig. 6 -

The H^- fraction of hydrogen scattered from a cesium surface as a function of the normal velocity component of the scattered particles. The turning point of the trajectory is at $z_o = R_{Cs^+} + R_{H^-} \approx 5\ a_o$. See also the capture of fig. 5.

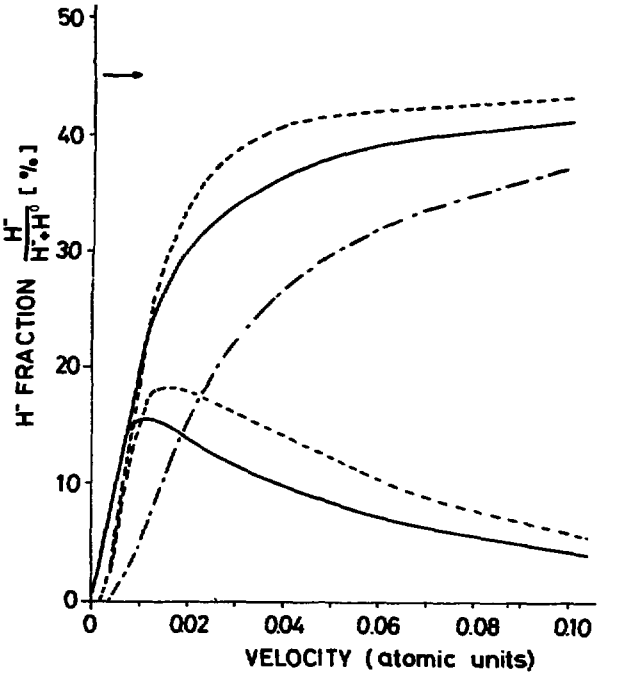

Fig. 7 -

The H^- fraction of hydrogen scattered from a partially with cesium covered tungsten surface ($\theta_{Cs} \approx 0.5$). The turning point of the trajectory is at $z_o = R_{Cs} + R_{H^-} \approx 5\ a_o$. See also the capture of fig.5.

In these calculations the functional dependence of the electron affinity and of the transition rate on the distance shown in figs. 3 and 4 are used. It turns out that the final H^- charge fraction is strongly dependent on the work function. This can be understood in terms of the equilibrium charge state: increasing work function gives rise to a decreasing overlap between conduction band and affinity level. This smaller H^- equilibrium charge state will give rise, also in the case of a moving particle, to a smaller final H^- charge state. The velocity dependence can be understood in terms of the "freezing distance" approach, already suggested in [11]. The freezing distance, which is given by

$$z^*(v_z) = \frac{1}{a} \ln \frac{\Delta_o}{a v_z} \qquad (9)$$

where Δ_o and a describe the exponential decaying transition rate at large distances, may be interpreted as the distance where the equilibrium charge state is frozen. The final charge state can now approximately be given by

$$\beta^-(v_z) \simeq N^-(z^*) \qquad (10)$$

Beyond the freezing distance, the transition time $\tau \approx \omega^{-1}$ is so large compared to the residence time of the particle in a small space interval, that electron transition cannot occur any more. At the freezing distance there is a change from a situation where complete adiabatic adjustment to the equilibrium charge state takes place to a situation where the charge state cannot change any more A larger velocity will shift this freezing point closer to the surface, so that the equilibrium charge state increases; thus an increasing velocity will give rise to an increasing final charge state. For low velocities ($\lesssim$ 0 01 a.u.) a quantitative expression can be found by substituting equation (6) and (9) in (10). The final H^- charge state is then given by

$$\beta^-(v_z) \approx \frac{1}{\pi} \frac{a\, v_z}{2(\phi - S - \Delta E)} \qquad (11)$$

This expression shows a linear dependence of the H^- charge state on velocity which can also be seen in the calculations of figs. 5, 6, 7.
The second term of equation (8) is an exponential decay function which only contributes to the final charge state at high velocities

4. THE AMPLITUDE MODEL

A more complete approach to incorporate the atom motion is given by Bladin et al. [12] and is worked out in more detail by Norskov et al [20]. The main difference between both models is that in the semiclassical model the time evolution of the probability for H^- formation is considered, while in the *quantum mechanical* model the time evolution of the corresponding wave function amplitude is considered. In the quantum mechanical model the final charge state at infinite distance from the surface is given by

$$\beta^-(v_z) = \frac{1}{\pi} \int_{-v_o}^{\infty} d\varepsilon\; f(\varepsilon,T) \left| \int_o^{\infty} \sqrt{\tfrac{1}{2}\Delta(t')}\, e^{-i\varepsilon t' - \int_t^{\infty} [i(-S-\Delta E(t'')) + \frac{1}{2}\Delta(t'')]\, dt''} dt' \right|^2 + P_o(o)\; e^{-\int_o^{\infty} \Delta(t')\, dt'} \qquad (12)$$

where $P_i(o)$ is again the charge state at the turning point and t is the time defined with respect to the turning point,

$$f(\varepsilon,T) = \frac{1}{1 + e^{-(\varepsilon+\phi)/kT}}$$

is the Fermi function, $\Delta E(t)$ and $\Delta(t)$ are the shift and broadening of the affinity level as a function of time, respectively. The numerical solution of equation (12) for W(110), cesiated W(110) and cesium are shown in figs. 5, 6, 7. For the level shift and width the same values are chosen as used in the semiclassical calculations From figs. 5, 6, 7 it is seen that especially for low velocities there is a remarkable difference between the semiclassical and the quantummechanical theory

Before proceeding first the charge state of a stationary atom is considered The equation (12) reduces for zero temperature now to

$$\beta^- \simeq \frac{1}{\pi} \int_{-v_o}^{-\phi} \frac{\Delta/2}{(\epsilon + S + \Delta E)^2 + \Delta^2/4} \, d\epsilon$$

which is equal to N^- the equilibrium charge state at that distance In the semi-classical model this limit has the same value. However, for low velocities it can be shown [12] that equation (12) reduces to

$$\beta^-(v_z) \simeq \frac{2}{\pi} \exp[-\pi(\phi - S)/2\ a v_z]$$

where a is the exponential decay constant of the transition rate at large distances. This low velocity limit is different from the linear behaviour of β^- on the velocity in the probability model. This deficiency of the probability model is due to the neglect of interference effects, which especially in the low velocity limit influences the final charge state distribution. The exponential decay term appears in both theories.

5. CONCLUSIONS

The negative ionization of hydrogen on metal surfaces is described by first determining the position of the affinity level and the transition rates Hereafter two methods to include the atomic motion are discussed and compared: a proba-

bility method in which the dynamics are described by a probability equation, and an amplitude method in which the dynamics are described by a time dependent amplitude equation. For not too low velocities and not too high work functions the results of both theories do not differ very much. For proton scattering on cesiated tungsten a good agreement between both theories and experimental results [5], concerning the maximum H^- yields, could be achieved. It should be noted, however, that in the calculations of H^+ to H^- conversion on surfaces it is also important to consider the particle and energy reflection coefficients.

APPENDIX

The one-electron wave function for the H^--ion:

The Schrödinger equation for the H^- ion is:

$$[-\tfrac{1}{2}(\Delta_1 + \Delta_2) - \frac{1}{r_1} - \frac{1}{r_2} + \frac{1}{r_{12}}]\ \psi(\vec{r}_1,\vec{r}_2) = E\ \psi(\vec{r}_1,\vec{r}_2) \qquad \text{(A1)}$$

At large distances of the nucleus, this two-electron equation can be reduced to a one-electron equation [21]. The solution gives the asymptotic form of the one-electron H^- ion wave function, the radial part of which is:

$$\phi(r) = \frac{A\ e^{-\sqrt{2S}\,r}}{r} \qquad \text{(A2)}$$

where $A = (2\sqrt{2S})^{\frac{1}{2}}$ is the normalization constant and S the affinity energy. At smaller distances, we may not use this expression which is diverging. As we have emphasized, the most important characteristic of our wave function is the one-electron radial density distribution defined by [22]:

$$D(r_1) = 2 \int_0^\infty [\iint \psi^*(\vec{r}_1,\vec{r}_2)\ \psi(\vec{r}_1,\vec{r}_2)\ d\Omega_1 d\Omega_2\ ]\ r_1^2 r_2^2 dr_2$$

where

$$d\Omega_i = \sin\theta_i d\theta_i d\phi_i$$

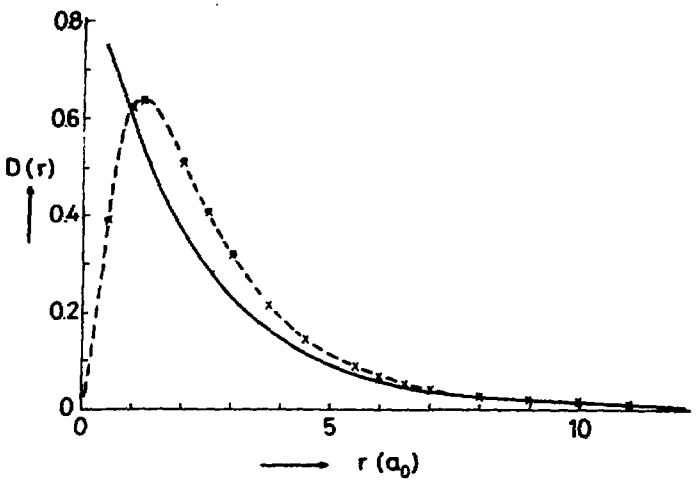

Fig. 8 - One-electron radial density distribution for the H^- ion.

——— *Asymptotic form (A2).*

----- *Green et al.;*

xxxxx *Points obtained with our fitted wave function.*

For getting a good description of $D(r_1)$ which is valid over the whole space, we use the correlated wave function of Green et al. [23] up to 6 a_o and the asymptotic form (A_2) beyond 6 a_o (fig. 8) and by applying the least square method fit the resulting curve by an adjustable wave function $\psi(r_1,r_2) = \phi(r_1)\phi(r_2)$. The resulting normalized one-electron wave function $\phi(r)$ is found to be:

$$\phi(r) = \sum_{i=1}^{3} a_i \, e^{-b_i r} \qquad \text{(A3)}$$

where in atomic units:

$$a_1 = 1.023,\ a_2 = 0.3857,\ a_3 = 0.03521,$$

$$b_1 = 1.259,\ b_2 = 0.4804,\ b_3 = 0.2370.$$

REFERENCES

[1] K.H. Berkner, R.V. Pyle, J.W. Stearns, Nucl.Fusion 15 (1975) 249.

[2] K. Wiesemann, K. Prelec, Th. Sluyters, J.Appl.Phys. 48 (1977) 2668.

[3] P.J. Scheider, K.H. Berkner, W.G. Graham, R.V. Pyle, J.W. Stearns, Proc.Symp.on Production and Neutralization of Negative Hydrogen Ions and Beams, Brookhaven, 1977.

[4] P. Massmann, H.J. Hopman, J. Los, XIVth Conf.on Phenomena in Ionized Gases, Grenoble, July 1979.

[5] J.N.M. van Wunnik, B. Rasser and J. Los, Phys.Letters 87A (1982) 288.
J. Los, E.A. Overbosch and J.N.M. van Wunnik, Proc.2nd Int.Symposium on the Production and Neutralization of Negative Hydrogen Ions and Beams, Brookhaven, 1980.

[6] N.D. Lang, A.R. Williams, Phys.Rev.Letters 34 (1975) 531; Phys.Rev. B 18 (1978) 616;
J.K. Norskov, Phys.Rev. B 20 (1979) 446.

[7] J.R. Hiskes, XIVth Int.Conf.on Phenomena in Ionized Gases, Grenoble, July 1979.

[8] R.K. Janev and S.B. Vojvodic, J.of Phys.B: Atom.Molec. Phys. 13 (1980) 2481.

[9] R.K. Janev, Surf.Sci. 45 (1974) 609.

[10] B. Rasser, M. Remy, Surf.Sci. 93 (1980) 223.

[11] E.G. Overbosch, B. Rasser, A.D. Tenner, J. Los, Surf.Sci. 92 (1980) 310.

[12] A. Bladin, A. Nourtier and D. Hone, J.Phys.(Paris) 37 (1976) 369.

[13] S. Horiguchi, K. Koyama and Y.H. Ohtsuki, Phys.Stat.Sol. (6) 87, 757 (1978).

[14] J.K. Norskov, D.M. Newns and B.I. Lundqvist, Surf.Sci. 80 (1979) 179.

[15] R. Gomer and L.W. Swanson, J.Chem.Phys. 38, (1963) 1613.

[16] N.D. Lang and W. Kohn, Phys.Rev. B 1 (1970) 4555.

[17] K.F. Wojciechowski, Surf.Sci. 55 (1976) 246.

[18] J.N.M. van Wunnik, J.C.C. Geerling, J. Los, Surf.Sci. to be published; this thesis chapter V.

[19] J.W. Gadzuk, Surf.Sci. 6 (1967) 133 and 159;
M. Remy, J.Chem.Phys. 53 (1970) 2487.

[20] J.K. Norskov, B.I. Lundqvist, Phys.Rev.B 19 (1979) 5661.

[21] H.A. Bethe, E.E. Salpeter, Quantum mechanics of one- and two-electron atoms, Springer-Verlag, 1957.

[22] K.E. Banyard, J.Chem.Phys. 48 (1968) 2121.

[23] L.C. Green, S. Matsushima, C. Stephens, E.K. Kolchin, M.H. Kohler, Y. Wang, B.B. Baldwin, R.J. Wisner, Phys. Rev. 112 (1958) 1187.

CHAPTER III

The Velocity Dependence of the Negatively Charged Fraction of Hydrogen Scattered from Cesiated Tungsten Surfaces

ABSTRACT

By scattering protons under grazing angles of incidence at a cesiated tungsten W(110) surface, the dependence of the scattered H^- fraction as a function of the normal and parallel velocity components is measured. The incident energy is ranging from 400 eV to 2000 eV, the angle of incidence is 80^o with respect to the surface normal. The experiments are done with a surface which is covered with half a monolayer cesium and a thick layer of cesium, corresponding to work functions of 1.45 eV and 2.15 eV respectively. The measurements show a strong dependence on the normal as well as the parallel velocity component.

The normal velocity component dependence can be understood in terms of the probability model. We extended this model to incorporate the parallel velocity. The essence of this extension is that the finite velocity of the metal electron is taken into account. Good agreement between theory and experimental results is obtained.

1 INTRODUCTION

In recent years there is an increasing interest in the formation of negative hydrogen ions by surface processes. This interest has a fundamental as well as a practical basis. The fundamental interest will be elucidated first.

To explain the interaction of hydrogen atoms with a metal two different models are applied. The first model makes use of the local density functional approximation, which gives information about the electron density distribution, the dipole moment and the heat of adsorption [1,2]. The validity of this theoretical approach ranges from inside the bulk till about 3 a_o in front of the surface. In the second model the atom-metal interaction is considered as a perturbation of the pure atomic and metal states. This model was first proposed by Gurney [3] and is later worked out by Gadzuk [4] for the chemisorption of alkalis on metal surfaces. For the determination of the fraction of negative hydrogen ions in front of a surface, Rasser et al. [5] showed that the same approach as used for the chemisorption of alkalis on metals can be used. The perturbational approach is valid for distances larger than 3 a_o. Both approaches handle problems in which the adatom is at a fixed distance from the surface. Only very recently theoretical approaches for a system in which the adatom moves with respect to the surface are developed.

One of the first attempts to describe the charge state of hydrogen scattered from a metal surface is made by Hiskes [6]. He distinguishes two separate regions in front of the surface. According to his assumptions the H^- ion is formed close to the surface, while at larger distances H^- decays partly to neutral hydrogen. The survival of H^- is assumed to be exponentially dependent on the velocity. However, in this empirical description neither the broadening of the hydrogen affinity level nor the metallic nature of the substrate is taken into account. A different approach is suggested by Overbosch et al. [7] and by Rasser et al. [5], which is based on a more sophisticated model. They calculate the electron transition frequency as a function of distance to the surface. Assuming a Fermi Dirac

distribution for the electrons in the free electron metal, they then derive a rate equation which describes the evolution of the negative charge fraction of the atoms as a function of the distance to the surface. Recently a third approach is suggested by Brako et al. [8] and by Norskov et al. [9]. Here not the time evolution of the probability is derived as in the approach of Overbosch et al. and Rasser et al., but the time evolution of the amplitude of the wave function. Rasser et al., however, showed that for low work function metals there is, except for very low velocities ($< 1.0 \ 10^4$ m/s), almost no difference between the results of both theories.

In these models it is always assumed that only the normal velocity component is the parameter which determines the final charge distribution. However, as already suggested by Van Wunnik et al. [10] and by Von Gemmingen et al. [11], because of the finite velocity of the metal electrons, also the parallel velocity component plays an important role.

In this paper we will follow the semi-classical theory of Overbosch et al. and of Rasser et al., however, taking into account the influence of the parallel velocity component.

The practical interest in H^- formation on surfaces is connected with plasma fusion experiments. For heating plasmas to ignition temperatures high energetic neutral hydrogen beams are needed which can be made by using H^- as an intermediate ion [12]. Another application is also found in plasma experiments. To determine the plasma temperature one can measure the energy distribution of the neutral atoms emitted by the plasma. For electrostatic energy analysis below 1000 eV one can convert the neutral atoms efficiently into negative ions by means of a negative surface ionization process. Massmann et al. [13] have shown that such a neutral particle analyser is in principle feasible.

Until recently the experimental studies were mainly focused on these applications. Schneider et al. [14] measured the yield on backscattered H^- when a proton beam hits under normal incidence a cesium surface. In the experiments of Massmann et al. [13] the same was done for a hydrogen ion beam under 45° with the surface normal. He used a substrate of thorium oxyde. In

both experiments the H^- yield is a convolution of the reflection coefficient and the charge transfer probability. Maximum efficiencies of 10% resp 7% were measured. To increase this yield Van Wunnik et al. [10] used a cesiated tungsten surface and changed to grazing angles of incidence to enhance the reflection coefficient. Now a maximum H^- yield of 40% could be measured. From these measurements it also became clear that not only the normal velocity component determines the charge state but also the parallel one.

Other ways of producing H^- are reported by Graham [15] who applies a cesium ion beam to sputter H^- from a hydrogen loaded surface and by Yu [16] who sputters H^- with Ne from a molybdenum surface which is loaded with hydrogen and cesium.

In all these experiments, however, no clear separation between reflection coefficient or sputter ratio and H^- formation probability can be made A first attempt to measure exclusively the H^- formation is performed by Eckstein et al. [17]. They measured the fraction of H^- in the outgoing trajectory with respect to all the scattered particles as a function of the energy of the scattered particles at a fixed scattering angle. The experiments were done on a cesiated Ni single crystal under normal incidence. The scattering angle was 45° with respect to the surface normal. In this case however no clear separation between the normal and parallel velocity component can be made because both components change with varying energy.

Von Gemmingen et al. [11] did this type of experiment under grazing angles of incidence with Cu and Ni crystals. These materials give rather low H^- yields (< 1.0 %). Because here the detection angle is also under grazing angles, the parallel velocity component is almost completely determined by the primary energy and not by the detection angle. So a separation between parallel and normal velocity component can be made. From these experiments also Von Gemmingen could conclude that besides the normal velocity also the parallel velocity component is an important parameter.

In this paper we report measurements of the H^- fraction in the outgoing trajectory for grazing angles of incidence and reflection The target is a cesiated tungsten (110) single

crystal; two cesium coverages are applied: half a monolayer which corresponds to a work function of 1.45 eV and a thick layer corresponding to a work function of 2.15 eV. The energy regime ranges from 400 eV to 2000 eV. The angle of incidence is 80° with respect to the surface normal and the detection angle varies from 70 to 90°. We use protons as primary particles.

In section 2 the model which incorporates the parallel velocity is explained. In section 3 the apparatus is described. The experimental results are discussed in section 4 from which some conclusions are drawn in section 5. The equations in this paper will be expressed in atomic units.

2. THEORETICAL

When a proton with an energy between 100 to 2000 eV approaches a surface it will be neutralized [18]. This neutralization process can be a direct Auger transition into the ground state of the atom. This transition occurs at distances of a few a_o. More probable for low work function materials, however, is first resonant neutralization in an excited state at a distance of approximately 10 a_o from the surface, followed by Auger deexcitation into the ground state of the atom at a distance of a few a_o. After this neutralization reflection on the surface occurs. It will be shown in the accompanying paper [19] that even for angles of incidence between 75° and 85° with the surface normal most of the particles will penetrate the cesium layer and reflect on the underlying tungsten surface.

Rogers et al. [20] showed that an atomic state cannot exist in the metal if the screening length of the metal is smaller than the radius of the atomic state. In low electron density materials like cesium (screening length approximately 1.5 a_o) this means that a neutral hydrogen state can exist but no negative hydrogen state. Negative hydrogen formation occurs after the atom has left the cesium layer. The radius of the negative hydrogen ion is of the order of 2 a_o. We shall assume that a negative hydrogen ion can exist when the separation be-

tween nucleus and surface is at least 2 a_o. In the outgoing trajectory there is now a probability for the neutral atom to become a negative ion over a normal distance of approximately 10 a_o

The negative hydrogen formation process has already been described by several authors [5,6,9]. However, in all of these models only the normal velocity component of the outgoing particles was assumed to be the charge determining factor. In this paper we also take into account the parallel velocity. This is done within the probability model described by Rasser et al. [5]. In a following publication the problem will be treated within the more complete amplitude model, which model was first proposed by Blandin et al. [21].

2.1. The negative hydrogen formation probability as a function of normal velocity

When a hydrogen atom is close to a metal surface, the affinity level is lower than the -0.75 eV in the case of a free hydrogen atom. This decrease is due to the induction of a positive image charge in the metal. Far from the surface (> 10 a_o) the shift can be described by the classical image potential equation.

$$\Delta E = - \frac{1}{4Z} \qquad (1)$$

where Z is the atom surface distance. Closer to the surface the finite screening length of the metal [22] and the polarizability of the atom give rise to a downward level shift which is less than the shift described by equation (1). The precise deviation from the classical image potential is, however, not well known.

For very small distances (< 3 a_o) Lang et al. [23] showed that if the metal is assumed to be a jellium metal the affinity level follows the effective potential of the metal. In the following we will approximate the surfaces under consideration as surfaces of jellium metals. The affinity level positions

for cesium and cesiated tungsten surfaces respectively are illustrated in figure 1. The position of the level between 4 and 11 a_o is determined empirically by a trial and error method. A certain start position will give in the H (H^+) - H^- conversion probability calculations rise to a certain conversion probability. By changing the level position within small limits the calculated conversion probabilities can be made equal to the measured ones.

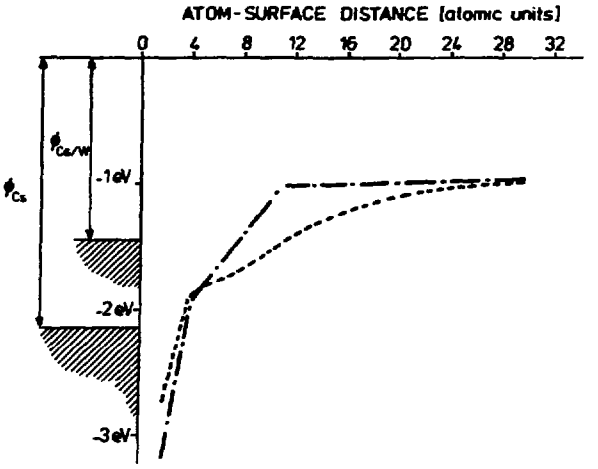

Fig. 1 - The position of the affinity level as a function of the atom-surface distance. -.-.-.- is the level position for a partially cesium covered tungsten (110) surface (ϕ = 1.45 eV). ------ is the position for a totally cesium covered surface (ϕ = 2.15 eV).

Fig. 1 shows that the affinity level can shift to energies around or even below the Fermi energy. This level shift together with the finite width of the potential barrier between conduction band and affinity level allows resonant transitions between the conduction band and the affinity level.

In principle the resonant transfer of electrons between a metal surface and an atom, which has a stable negative ion state, is a two-electron problem. In case of hydrogen, however,

the separation between the ionization level and affinity level is so large, that the neutralization respectively formation of a negative ion can be considered to be uncorrelated The transition matrix element is given by [4,5]:

$$T_{\vec{k}i}(Z) = \langle \vec{k} | V | i \rangle \tag{2}$$

in which $|\vec{k}\rangle$ is the metallic state, $|i\rangle$ the negative ion state and V the unperturbed core potential of the neutral atom. For a more detailed discussion we refer to Rasser et al. [5]. The total transition rate is the sum of the transition rates of the individual metal states, where these states must be in resonance with the atom affinity level. So the total transition rate is

$$\omega(Z) = 2\pi \sum_{\vec{k}} |T_{\vec{k}i}(Z)|^2 \, \delta(E_{\vec{k}} - E_a(Z)) =$$

$$= 2\pi \sum_{\text{deg}} \rho(E_a(Z)) \, |T_{\vec{k}i}(Z)|^2 \tag{3}$$

Here $\rho(E_a(Z))$ is the density of states in the metal at the position of the affinity level. The sum has to be taken over all the degeneracies of the metallic states. The metal wave functions and the density of states are determined in the framework of the free-electron model for the metal.

$$E_{\vec{k}} = \tfrac{1}{2} |\vec{k}|^2 \tag{4}$$

The transition rate gives rise to a finite lifetime of the state which means a Heisenberg broadening of the affinity level. The width of the level is given by

$$\Delta(Z) = \omega(Z) \tag{5}$$

The metal states, which are in resonance with the affinity level are Lorentz distributed [24] around the metal states with $E_{\vec{k}} = E_a$. Here E_a is the position of the affinity level and $E_{\vec{k}}$ the energy of the metal state $\vec{k}$. The half width of this distribution in the $\vec{k}$ space is given by $\sqrt{\Delta}/k_a$. These resonan-

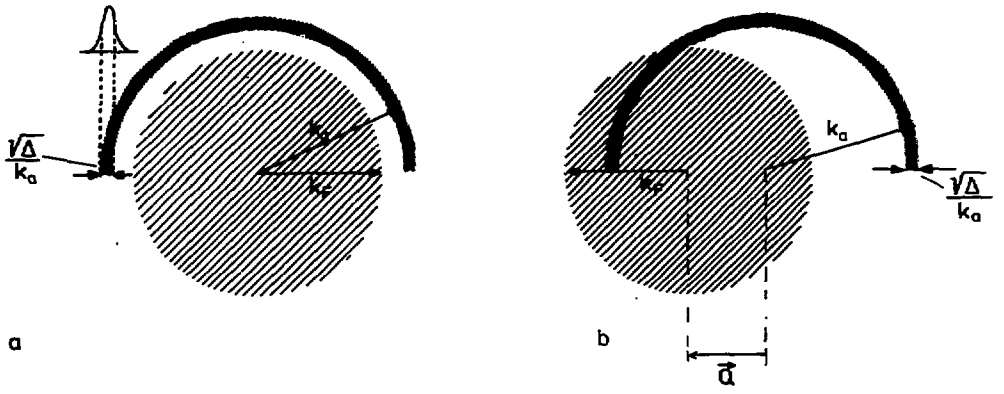

Fig. 2a - Schematic view of the metal $\vec{k}$ space. The shaded circle indicates the Fermi sphere. The dotted (half)ring indicates the metal states which are in resonance with the affinity level. Position and bandwidth of the affinity level correspond to respectively radius and width of the dotted ring. If the atom-metal distance decreases, the position of the affinity level shifts to lower energies and the width of the level becomes larger, the radius of the ring will decrease and the width of the ring will become larger. The overlap between the dotted ring and the circle determines N^-. In this scheme the parallel velocity is zero. $\frac{1}{2} k_F^2$ gives the position of the affinity level with respect to the bottom of the conduction band. $\frac{1}{2} k_F^2$ gives the position of the Fermi level.

Fig. 2b - In this scheme the parallel velocity is not zero. The overlap between the dotted ring and the shaded circle is changed with respect to figure 2a and so N^- will be different. $\vec{Q}$ is the additional momentum of the metal electrons seen from the moving atom.

ce states are indicated by the shaded area in fig. 2a. The behaviour of the level width as a function of distance for cesiated tungsten is shown in fig. 3.

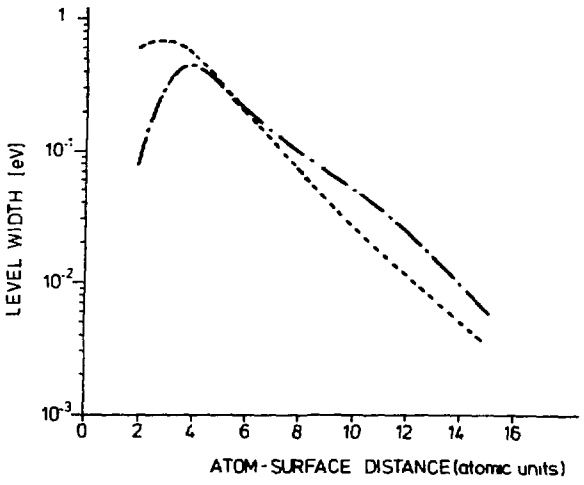

Fig. 3 -

The level width as a function of atom-surface distance. -.-.- is the level width for a with half a monolayer cesium covered tungsten (110) surface (ϕ = 1.45 eV). ---- is the level width for a thick cesium layer (ϕ = 2.15 eV).

From the position of the affinity level and the level broadening, one can now determine the fraction of the hydrogen particles (N^-) which are negatively charged at a given distance Z from the surface. N^- is that fraction of the total transition rate which is determined by filled metal states. N^- can be obtained from:

$$N^-(Z) = \frac{\sum_{\vec{k}} |T_{\vec{k}i}(Z)|^2 \, L(E_{\vec{k}}, E_a(Z), \Delta(Z)) \, f(E_{\vec{k}}, E_F, T)}{\sum_{\vec{k}} |T_{ki}(Z)|^2 \, L(E_{\vec{k}}, E_a(Z), \Delta(Z))} \qquad (6)$$

Here $L(E_k, E_a(Z), \Delta(Z))$ is a Lorentz distribution with halfwidth $\Delta(Z)$ at the affinity level position and $f(E_{\vec{k}}, E_F, T)$ the Fermi distribution of the metal electrons with temperature T. The summation is taken over all metal states. Fig. 4 shows the behaviour of N^- as a function of distance from the surface.

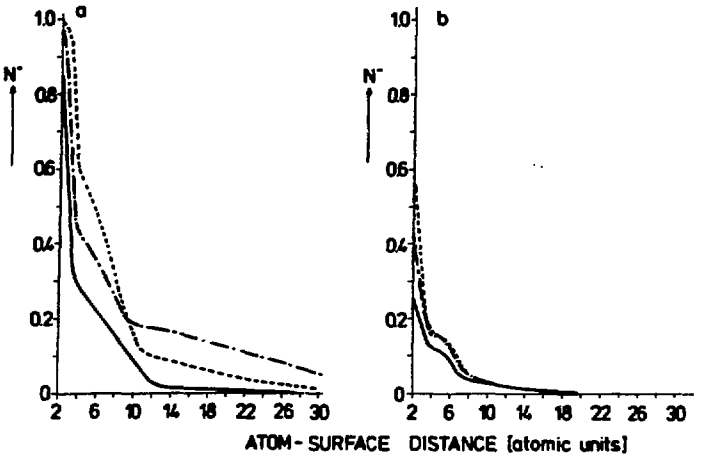

Fig. 4a - The fraction of negatively charged particles at a given distance from the surface (N^-) as a function of the atom-surface distance. The parallel velocity is resp. ------ 2.8 10^5 m/s (400 eV), -.-.- 4.5 10^5 m/s (1000 eV), and ——— 6.3 10^5 m/s (2000 eV). The work function is 1.45 eV.

Fig. 4b - N^- as a function of the atom-surface distance. The work function is 2.15 eV. See also the caption of figure 4a.

Before determining the fraction of negatively charged ions at an infinite distance from the surface, we first consider the time evolution of the system when the atom is at a given distance from the surface. Here we assume a charge distribution which is not equal to N^-. The time evolution of the charge state is then described by the rate equation:

$$\frac{dP_i(t)}{dt} = \Delta(Z)\ [N^-(Z) - P_i(t)] \qquad (7)$$

Here $P_i(t)$ is the actual charge state of the system at time t.

For a moving particle we can transform this time dependent rate equation to a distance dependent equation by making use of the time to distance relation of the particles with respect to the surface. For a straight line approximation of the outgoing trajectory we get

$$Z = Z_o + v_\perp t \tag{8}$$

where $v_\perp$ is the normal velocity component and Z_o the smallest distance from the surface where the particle can exist as H^-. Equation (7) is easily converted into

$$\frac{dP_i(Z)}{dZ} = \frac{A(Z)}{v_\perp} [N^-(Z) - P_i(Z)] \tag{9}$$

The final fraction of negatively charged ions can be determined by integrating formula (9) from Z_o to infinity. The final negative charge fraction is then given by

$$\beta^-(v_\perp) = \frac{1}{v_\perp} \int_{Z_o}^{\infty} A(Z)\ N^-(Z)\ \exp(-\frac{1}{v_\perp} \int_{Z}^{\infty} A(Z')\ dZ')\ dZ \tag{10}$$

2.2 Dependence of the negative hydrogen ion formation probability on the parallel velocity

In the model described so far, no dependence on the parallel velocity is included. To do this we first show that the position of the affinity level in our energy regime, 100 eV to 2000 eV, is not changed because of the parallel velocity.

The affinity level position is determined by the screening image charges in the metal surface. To investigate whether these charges are still formed or not when the particle is moving along the surface, we use the classical electrodynamic arguments formulated by Boyer [25]. He showed that screening of a moving charge still takes place when

$$\frac{\eta\ v_\parallel}{d} << 1 \tag{11}$$

Herein η is the resistivity of the surface. For the cesiated tungsten surface under consideration we take the resistivity of bulk cesium which is equal to 18.8 10^{-8} ohm m. As surface distance d is taken the smallest distance where a negative hydrogen ion can exist, that is $2a_o$. The left hand side of eq. (11) now yields for a parallel velocity corresponding to a hydrogen energy of 2000 eV a value of 1.0 10^{-2}. So we can assume the affinity level position to be independent of the parallel velocity in the energy regime considered.

On the other hand one can compare the maximum electron velocity in the metal with the parallel velocity of the hydrogen atom. The width of the conduction band in cesiated surfaces is of the order of 2 eV. This corresponds to a maximum electron velocity of 8.5 10^5 m/s. A hydrogen atom with an energy of 2000 eV has a velocity of 6.5 10^5 m/s, which is of the same order as the maximum electron velocity in the metal. To make a transition to the atom, a single metal electron needs approximately the same velocity parallel to the surface as the parallel velocity of the atom. For zero parallel velocity the largest number of metal electrons can make a transition. At a hydrogen velocity of 6.5 10^5 m/s, however, there are considerably less metal electrons able to make the transition. So for particles moving parallel to the surface the charged fraction will be smaller than for particles with parallel velocity zero. We can summarize that on the one hand the collective effect of the metal electrons is fast enough to screen the moving ion, but on the other hand the individual velocity of the electrons is not large enough to allow a transition.

For a more detailed picture we have to consider the way N^- is determined. It does not matter whether the transition process is considered in the reference frame of the metal or the one of the atom. For simplicity we shall look at the problem from the point of view of the atom.

If the atom is fixed and the metal is moving with a velocity $\vec{v}_{\|}$, the metal electrons will get an additional velocity $\vec{v}_{\|}$. The momentum of an electron with a momentum vector $\vec{k}$ in the metal frame then will become $\vec{k} + \vec{Q}$, where $\vec{Q}$ is in atomic units

equal to $\vec{v}_{||}$. In other words: the Fermi sphere will be shifted by $\vec{Q}$ in $\vec{k}$ space (see fig. 2b). The transition rate is unaffected by this shift because this rate is only determined by the number and position of states which are resonant with the affinity level and not by the fact whether these states are filled or not. The value of N^-, however, will change. N^- again is determined by eq. (6), but because the overlap between the states which are in resonance and the filled states, is changed (see figure 2b), N^- in most cases will be smaller than in the case $\vec{v}_{||}$ is zero. Fig. 4a and b show the dependence of N^- on the parallel velocity and distance determined by the eq. (6). In this figure we see that for small surface distances N^- indeed dramatically decreases, however for distances larger than 10 a_o a small increase of N^- is possible. This increase is due to the fact that for distances larger than 10 a_o in the case $\vec{v}_{||} = 0$, the states which are in resonance with the affinity level are far out of the Fermi sphere and so N^- is very small. For non-zero values of $\vec{v}_{||}$, however, an overlap between states in the Fermi sphere and resonant states can take place, and so for these distances N^- can increase with parallel velocity.

The precise shape of the $N^-(Z)$ curve is determined by the position of the affinity level as a function of the atom-surface distance The discontinuities in the $N^-(Z)$ curve have no physical meaning. They result from the discontinuities in the affinity level position curve which is chosen rather arbitrarily. The final negatively charged fraction of a hydrogen atom which leaves the surface with normal velocity $\vec{v}_\perp$ and parallel velocity $\vec{v}_{||}$ is again given by eq. (10). Here the parallel velocity dependence of N^- must be included.

3. APPARATUS

A complete description will be published in the accompanying paper [19]. We here confine ourselves to the main elements. The apparatus consists of an H^+ beamline and a UHV chamber. The energy of the H^+ beam can be varied between 100 eV and 10000 eV. The beam can be focused on a tungsten (110) target,

which is mounted in the centre of the UHV chamber. The beam opening angle at the target is of the order of 1.0° and the beam diameter is of the order of 1.0 mm. The beam current is 1.0 10^{-11} A. After reflection from the target the particles can be analysed with a parallel plate energy analyser. The central axis of the target coincides with the central axis of the UHV chamber. The target and the analyser can be rotated about this axis. The dimensions of the target are 2.0 × 15.0 × 0.2 mm. The analyser serves to measure the angular and energy distribution of the scattered particles and can also be used to determine the fraction of the scattered particles which is negatively charged. When no voltages are applied to the analyser all particles within an opening angle of 0.5° hit a channeltron. If however analysing voltages are applied to the plates the charged particles will be deflected and only neutral particles are collected by the channeltron. To determine the charged fraction at 400 eV, 1000 eV and 2000 eV as a function of the scattering angle we use the channeltron detection efficiencies for H and H^-, measured by Crandall et al. [26]. The fraction of H^+ over H^- can be derived by comparing the absolute intensity of the energy spectra of both particles.

The tungsten target can be ohmically heated up to 2700 K. The target is cleaned by standard oxygen treatments [27]. The target can be covered with cesium by means of a cesium dispenser (obtained from SAES GETTERS, Italy) mounted 1 cm in front of the target. The surface is checked by LEED and Auger measurements and the work function of the surface is measured with a Kelvin probe. The working pressure in the UHV system is 1.0 10^{-9} Torr.

4. RESULTS AND DISCUSSION

The negatively charged fraction of the scattered particles as a function of scattering angle, total energy and cesium coverage of the tungsten target is shown in fig. 5 and 6. The angle of incidence is 80° and the detection angle is varied from 70° to 90°. Comparison of the intensities of the energy

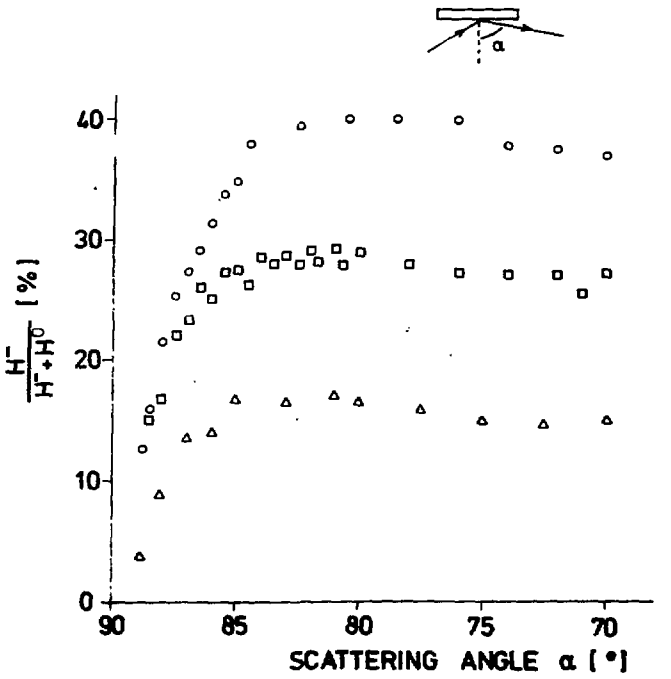

Fig. 5 - The H^- fraction of the scattered particles as a function of the scattering angle. The surface is partially cesium covered tungsten (110). The work function is 1.45 eV. The data points are indicated by OOOOO for 400 eV, □□□□□ for 1000 eV and ΔΔΔΔΔ for 2000 eV. The angle of incidence is 80° with the surface normal.

spectra of H^+ and H^- shows that the amount of H^+ is less than 1% of the scattered H^- ions. In the following we shall therefore neglect the H^+ ions.

Because of the grazing angles the parallel velocity stays almost unaltered when the detection angle is varied. In figs. 7a and 7b the data are plotted versus the normal velocity component. Here it is assumed in the calculations of $v_\perp$ that for a given energy the parallel velocity is constant. The reflected particles have lost 5 to 10% of energy with respect to the primary particles [19]. This energy loss will not change the curves 7a and 7b essentially and is therefore neglected.

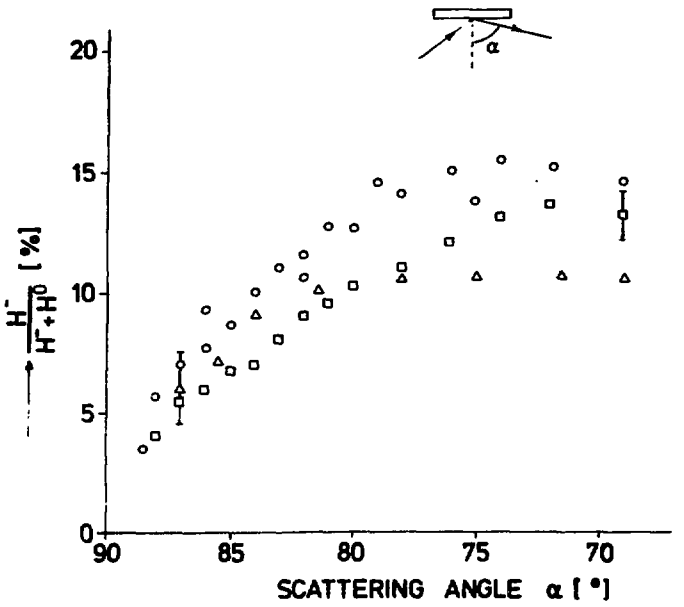

Fig. 6 - The H^- fraction of the scattered particles as a function of the scattering angle. The surface is a thick cesium layer (on a tungsten (110) surface). The work function is 2.15 eV. See also figure 5.

Another effect not taken into account is that particles leaving the surface lose about 1 eV of their normal energy because they are attracted by their own image force. The data points of the low normal velocities may therefore shift to higher values with a maximum shift of $1.5 \ 10^4$ m/s.

For very low normal velocities it can be seen that almost all the particles reflect as neutrals. For increasing normal velocity the negatively charged fraction increases and reaches a plateau. The height of this plateau decreases when the total energy, which means the parallel velocity, increases. In case of half a monolayer cesium ($\phi = 1.45$ eV) this decrease starts at 1000 eV, whereas for a thick cesium layer ($\phi = 2.15$ eV) the decrease begins at 2000 eV.

This behaviour is consistent with the total conversion ef-

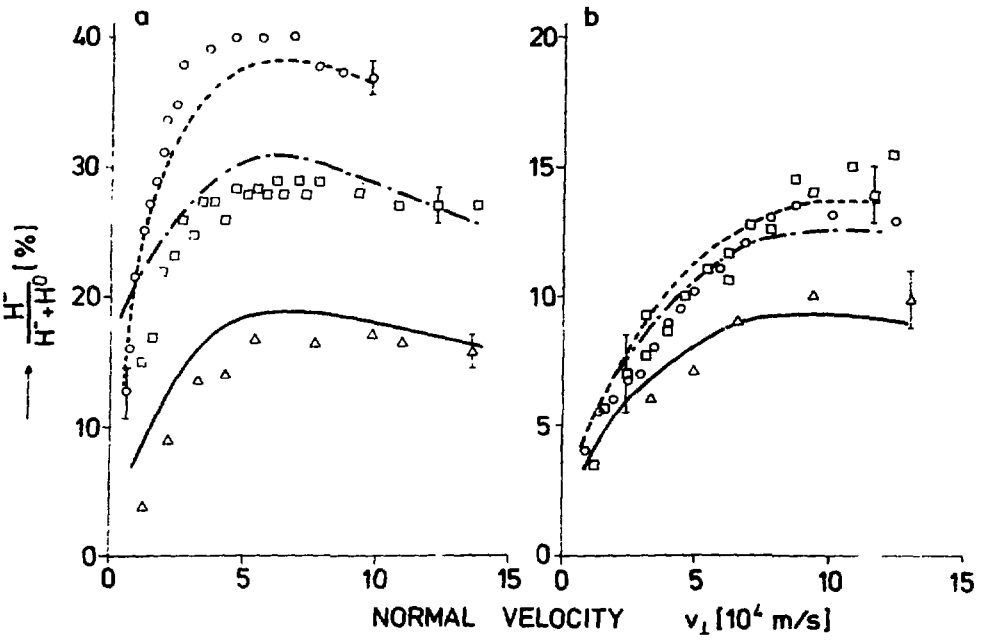

Fig. 7a - The H^- fraction in the scattered particles as a function of the normal velocity. The data points are indicated by OOOOO for 400 eV, by □□□□□ for 1000 eV and by ΔΔΔΔΔ for 2000 eV. The calculations are indicated by ----- for 400 eV, by -.-.- for 1000 eV and by ——— for 200 eV. The work function is 1.45 eV.

Fig. 7b - The H^- fraction in the scattered particles as a function of the normal velocity, for a with a thick cesium layer covered tungsten (110) surface. The work function is 2.15 eV.

ficiencies measured as a function of the angle of incidence by Van Wunnik et al. [10,19]. In the case of a partially cesiated tungsten (110) surface the maximum total conversion efficiencies measured for different incident energies (400 eV, 1000 eV, 2000 eV) roughly correspond to the height of the plateaus in figure 5 Comparative measurements with deuterium [10] show

that in this case the maximum conversion efficiency equals the value obtained for hydrogen of half the energy. This suggests already that also the parallel velocity is a determining factor for the height of the conversion efficiency.

For reflection at 400 eV and 1000 eV on thick cesium the parallel velocity is not a very sensitive parameter. Figure 7b shows now a scaling of the charge fraction with normal velocity for these energies.

In figure 7a and 7b the calculated curves using eq. (6) are also shown. These curves are calculated with work functions of 1.45 eV and 2.15 eV respectively. For the Fermi energy is chosen 1.95 eV and 1.57 eV, which is equal to the width of the conduction band at the centre of the cesium atoms. This width is equal to the effective potential at that position which can be determined by the procedures described in [5] and [28]. The position of the affinity level between 4 a_o and 11 a_o is determined with a fitting procedure. For 400 eV this position is adjusted to obtain good agreement with the measurements. For the other energies the same level positions are used. This procedure is carried out for half a monolayer as well as for a thick cesium layer.

A qualitative understanding of these results can be obtained applying the freezing distance model proposed by Overbosch et al. [7] and by Rasser et al. [5]. When a hydrogen atom leaves and is still close to the metal there will be a strong interaction between the atom and the metal. The transition time is very small compared to the time the atom spends in front of that surface. Therefore in that region the atom leaves the metal adiabatically. At each distance the equilibrium negative charge fraction N^- will be reached. However, far from the surface there is almost no interaction between the atom and the metal. The charge state will not change any more at these distances. As a consequence at an intermediate distance the so-called freezing distance, the charge state will be frozen. The N^- value established at this distance will be maintained till infinite distance from the surface. For very low velocities the particle stays in equilibrium with the surface over

very large distances and the freezing distance will be far out of the surface. With increasing normal velocity the adiabatic behaviour is the broken up closer to the surface and so the freezing distance shifts to smaller values. The final negative charge fraction for increasing velocities is more or less determined by the behaviour of N^- going from large to small distances. It is clear now that a decrease in N^-, because of an increasing parallel velocity, is connected with a decreasing final negative charge state.

On the other hand, for very large normal velocities $\langle v_\perp \rangle$ $2.0 \ 10^5$ m/s and fixed parallel velocity the freezing approach is no more a valid concept. For these velocities the region of H^- formation is transversed so fast that in the time the atom spends in this region less than one transition can be made. A transition becomes less probable with higher velocities. The negatively charged fraction as function of normal velocity, will, according to eq. (10), in first approximation be proportional to $1/v_\perp$ In the measurements of figure 5 and 6 this regime is not reached.

5. CONCLUSIONS

The figures 7a and 7b show a good agreement between theory and experiments. This indicates that in the regime where surface processes are important not only the normal velocity component is the final charge state determining parameter but, because of the finite velocity of the electrons in the metal, also the parallel velocity component.

As well as a $\vec{v}_{||}$ effect one can also expect a similar effect for the normal velocity. In the experiments shown, however, we always work with grazing angles, this implies that the normal velocity is not larger than $1.5 \ 10^5$ m/s which is negligible with respect to the Fermi velocity of $8.0 \ 10^5$ m/s.
For the applications of the H^- formation we can summarize that it is preferable to use low work function surfaces because they give conversion efficiencies up to 40%. On the other hand, low

work functions are almost always connected with a small conduction band width which gives already for low parallel velocity components a decrease of the negatively charged fraction. For hydrogen one can only get conversion efficiencies up to 40% for energies below 500 eV.

ACKNOWLEDGEMENTS

The authors wish to thank Prof.Dr. S.A. Wouthuysen for the fruitful discussions and for calling our attention to the importance of the finite velocity of the metal electrons.

This work is part of the research program of the Stichting voor Fundamenteel Onderzoek der Materie (Foundation for Fundamental Research on Matter) and was made possible by financial support from the Nederlandse Organisatie voor Zuiver-Wetenschappelijk Onderzoek (Netherlands Organization for the Advancement of Pure Research).

REFERENCES

[1] N.D. Lang and A.R. Williams, Phys.Rev.Letters 34 (1975) 531.

[2] J.P. Muskat and D.M. Newns, Phys.Review B 19 (1979) 1270.

[3] R.W. Gurney, Phys.Rev. 47 (1935) 479.

[4] J.W. Gadzuk, Surface Sci. 6 (1967) 133.

[5] B. Rasser, J.N.M. van Wunnik and J. Los, Surface Sci. 118 (1982) 697.

[6] J.R. Hiskes, 14th Intern.Conf.on Phenomena in Ionized Gases, Grenoble, 1979.

[7] E.G. Overbosch, B. Rasser, A.D. Tenner and J. Los, Surface Sci. 92 (1980) 310.

[8] R. Brako and D.M. Newns, Surface Sci. 108 (1981) 253.

[9] J.K. Norskov and B.I. Lundqvist, Phys.Rev. B19 (1979) 5561.

[10] J.N M. van Wunnik, B. Rasser and J. Los, Phys.Letters 87A (1982) 228.

[11] U. von Gemmingen and R. Sizmann, Surface Sci. 114 (1982) 445

[12] K H. Berkner, R V. Pyle and J W. Stearns, Nucl.Fusion 15 (1975) 249

[13] P. Massmann, H.J. Hopman and J. Los, Nucl.Instrum.Methods 165 (1979) 531.

[14] P.J. Schneider, K.H. Berkner, W G. Graham, R.V. Pyle and J.W. Stearns, Phys.Rev. B23 (1981) 941.

[15] W G Graham, Phys Letters 73A (1979) 186.

[16] M.L Yu, Phys Rev.Letters 40 (1978) 574.

[17] W Eckstein, H. Verbeek and R.S. Bhattacharya, Surface Sci. 99 (1980) 356.

[18] S. Horiguchi, K. Koyama and Y.H. Ohtsuki, Phys Status Solidi 87 (1978) 757.

[19] J N M. van Wunnik, J.J C. Geerlings, E.H.A. Granneman and J Los, published in the accompanying paper, this thesis chapter V.

[20] F.J. Rogers, H.C. Graboske and D.J. Harwood, Phys.Rev. A1 (1970) 1577.

[21] A. Blandin, A Nourtier and D. Hone, J.Physique 37 (1976) 369.

[22] R. Gomer and L.W Swanson, J.Chem.Phys. 38 (1963) 1613.

[23] N.D. Lang and A.R. Williams, Phys.Rev. B 18 (1978) 616.

[24] M Remy, J Chem.Phys. 53 (1970) 2487.

[25] T.H. Boyer, Phys.Rev.A 9 (1974) 68.

[26] D.H. Crandall, J.A. Ray and C. Cisneros, Rev.Sci.Instrum. 46 (1975) 562.

[27] J.A. Becker, E.J Becker and R.G. Brandes, J.Appl.Phys. 32 (1960) 411.

[28] K.F. Wojciechowski, Surface Sci. 55 (1976) 246.

CHAPTER IV

Incorporation of the Parallel Velocity Effect in the Amplitude Method

ABSTRACT

The negatively charged fraction in proton scattering at cesiated tungsten is experimentally found to be a strong function of the parallel ($\vec{v}_{\parallel}$) as well as the normal velocity ($v_{\perp}$). In the previous chapter the parallel velocity was included via the probability method. In that treatment the atom was fixed and the metal was moving. In this chapter we will include the parallel velocity via the amplitude method. Here, however, the metal is fixed and the atom is moving. As in the probability method also the amplitude method shows that $\vec{v}_{\parallel}$ may be taken into account by displacing the Fermi sphere in the existing theory by $\vec{Q} = \vec{v}_{\parallel}$. A simple model and a more complete calculation explain the H^+ scattering data.

1. INTRODUCTION

Charge exchange between atom or ion beams with surfaces in the energy range of a few eV to many keV is an increasingly studied phenomenon. Like in the closely related problem of the charged fraction of sputtered particles, it has intriguing theoretical aspects. In the case of atoms with a valence level near the substrate Fermi level the dominant mechanism for interchanging charge with the surface is direct hopping of electrons (resonant process), rather than Auger neutralization [1-5].

A readily available experimental result is the charged fraction of the scattered particles as function of the angle of incidence or reflection of the particles. For grazing incidence the change of the scattering angle will give, in the grazing scattering regime, information about the normal velocity dependence of the charged fraction. The parallel velocity is then in first approximation constant. Only increasing the incident energy will increase the parallel velocity. This way of separating the normal and the parallel velocity dependence seems to have been little applied. The experiments of chapter III, based on these ideas, show for H^- scattered from cesiated tungsten a strong parallel velocity effect (figure 1).

2. THEORETICAL

The closeness of the hydrogen affinity level to the Fermi level suggests operation of the resonant process. Our theoretical approach of this resonant charge transfer process will be on basis of the system atom-jellium. This jellium limitation is not too serious. At not too small ($\gtrsim 2\ a_o$) distances the atom couples most strongly to the free electron like sp-orbitals of the substrate. At reasonable low velocities ($v_\perp < 1.0\ \ 10^5$ m/s) the coupling at large distances is the most important, and so for these low velocities a jellium approximation seems justified.

We also will assume that the affinity level is the only level in interaction with the conduction band. In principle

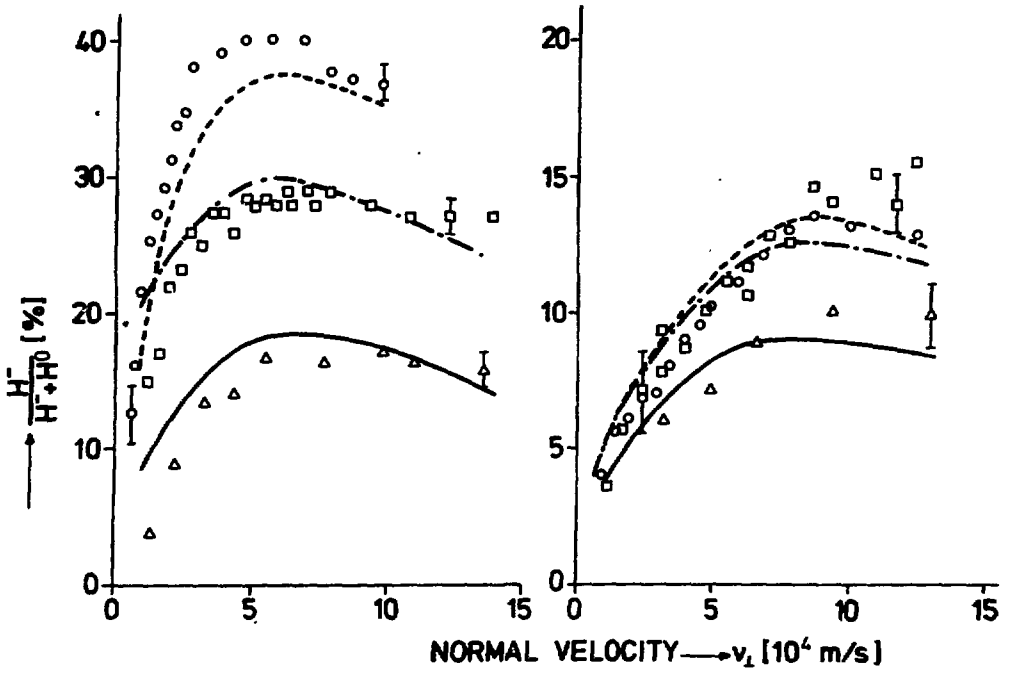

Fig. 1 - The H fraction of the scattered particles as function of the normal velocity. The data points are indicated by OOOOO for 400 eV (which corresponds to a parallel velocity of ≈ 2.8 . 10 ^{5} m/s) by □□□□□ for 1000 eV (≈ 4.5 . 10^5 m/s) and by ΔΔΔΔΔ for 2000 eV (≈ 6.3 . 10^5 m/s). The calculations are indicated by ----- for 400 eV, by -.-.- for 1000 eV and by ——— for 2000 eV. In figure 1a the work function is 1.45 eV, in figure 1b the work function is 2.15 eV.

the resonant charge transfer of electrons between a metal surface and an atom, which has a stable negative ion, is a two-electron problem. The separation between ionization and affinity level in case of hydrogen is so large, that the neutralization respectively formation of a negative ion can be considered to be uncorrelated.

The problem will be handled within an Anderson model framework, wherein one single orbital ψ_a mixes with the eigenstates $\psi_{\vec{k}}$ of the semi-infinite jellium.

The Hamiltonian for a single electron of momentum $\vec{p} = (\vec{p}_{||}, p_{\perp})$ and coordinate $\vec{x} = (\vec{x}_{||}, z)$ is

$$H = \frac{\vec{p}^2}{2} + V(\vec{x}_{||} - \vec{v}_{||}t,\ z - Z(t)) + V_{eff}(z) \qquad (1)$$

where $\vec{v}_{||}$ is the velocity parallel to the surface, assumed to be constant, Z the distance from the atom to the surface, V in the case of negative ionization the potential of the active electron in the neutral atom core and V_{eff} the effective potential of the jellium surface. V_{eff} is composed out of exchange and correlation terms of the free electron gas and of terms which account for the in the surface induced image charges by the in front of the surface situated "affinity" electron and atomic core. The expansion of the total wave function ψ in terms of pure metallic wavefunctions $\psi_{\vec{k}}$ and the atomic wavefunction ψ_a, where the atomic and metallic states are assumed to be orthonormal, is

$$\psi = \sum_{\vec{k}} c_{\vec{k}} \psi_{\vec{k}}(\vec{x}) + c_a\ U\ \psi_a(\vec{x}_{||}, z - Z(t)) \qquad (2)$$

U is the Galilean transformation operator

$$U = \exp[i\ \vec{v}_{||} \cdot \vec{x}_{||} - i\,t\,\vec{v}_{||} \cdot \vec{p}_{||}\ ] \qquad (3)$$

and is such that $U\ \psi_a(\vec{x})\ \exp(-iE_a(Z)t)$ is a solution of the time-dependent Schrödinger equation for an atom at Z moving with uniform velocity $\vec{v}_{||}$ parallel to the surface, with $E_a(Z)$ the energy eigenvalue of orbital ψ_a at Z.

The expansion (2) is substituted into the time-dependent Schrödinger equation belonging to (1)

$$i\ \frac{\partial \psi}{\partial t} = H\ \psi$$

When, multiplying by ψ_a or $\psi_{\vec{k}}$, integrating over all $\vec{x}$ and using the assumed orthogonality of the a and $\vec{k}$ states and the algebra of the $\vec{p}_{\|}$ and $\vec{x}_{\|}$ operators in (3), we obtain the Heisenberg equations of motion

$$i\,\dot{c}_a = E_a(t)\,c_a + \sum_{\vec{k}} c_{\vec{k}}\,\exp[i(E_{\vec{k}} - E_{\vec{k}-\vec{Q}})t]T_{(\vec{k}-\vec{Q})i}(t) \qquad (4)$$

$$i\,\dot{c}_k = E_{\vec{k}}\,c_{\vec{k}} + c_a\,\exp[-i(E_{\vec{k}} - E_{\vec{k}-\vec{Q}})t]T^{*}_{(\vec{k}-\vec{Q})i}(t) \qquad (5)$$

In eq. (4) and (5) $E_{\vec{k}}$ is the energy eigenvalue $\frac{1}{2}|\vec{k}|^2$ of $\psi_{\vec{k}}$, $E_a(t) = E_a(Z(t))$, $\vec{Q} = \vec{v}_{\|}$. The matrix element $T_{(\vec{k})i}$ is

$$T_{(\vec{k})i}(Z(t)) = \langle\vec{k}|V(\vec{x}_{\|}, z - Z(t))|i\rangle \qquad (6)$$

in which $|k\rangle$ is the metallic state and $|i\rangle$ the atomic state. Our aim is the calculate the expectation value

$$\langle n_a(\infty)\rangle = \langle c_a^{*}(\infty)\,c_a(\infty)\rangle \qquad (7)$$

of the charge in the affinity level at time $t \to \infty$, so for the measurements of $\langle n_a\rangle$ after the particle has left the metal.

We assume a separability between the $\vec{k}$ and t dependence of $T_{(\vec{k})i}(t)$

$$T_{(\vec{k})i}(t) = P_{\vec{k}}u(t) \qquad (8)$$

Now the $c_{\vec{k}}$'s may be eliminated [2,4] except for the operators $c^{o}_{\vec{k}}$ at an initial time t_o to give the basic integro-differential equation for c_a.

$$i\,\dot{c}_a = E_a(t)\,c_a + \sum_{\vec{k}} T_{(\vec{k})i}(t)\,\exp[-i(E_{\vec{k}}t - E_{\vec{k}+\vec{Q}}\,t_o]c^{o}_{\vec{k}+\vec{Q}}$$

$$- \frac{i}{2\pi}\int_{t_o}^{t} dt'\,u(t)u^{*}(t')\int_{-\infty}^{\infty} d\omega\, e^{-i\omega(t-t')}\,\Delta(\omega)\,c_a(t') \qquad (9)$$

where

$$\Delta(\omega) = 2\pi \sum_{\vec{k}} |P_{\vec{k}}|^2 \, \delta(\omega - E_{\vec{k}}) \tag{10}$$

In the case of a motion parallel to the surface at Z_c eq. (9) may be solved exactly to give

$$\langle n_a(Z_c)\rangle = \sum_{\vec{k}} \frac{f(E_{\vec{k}+\vec{Q}},\, E_F, T)\ |P_{\vec{k}}|^2}{|E_{\vec{k}} - E_a(Z_c) - \Lambda(E_{\vec{k}}) + i\,\tfrac{1}{2}\Delta(E_{\vec{k}})|^2} \tag{11}$$

$\Lambda(\omega)$ is the Hilbert transform of $\Delta(\omega)$ and $f(E_{\vec{k}+\vec{Q}}, E_F, T)$ the Fermi function.

$$f(E_{\vec{k}+\vec{Q}}, E_F, T) = \frac{1}{\exp[\dfrac{\frac{1}{2}|\vec{k}+\vec{Q}|^2 - E_F}{kT}] + 1} \tag{12}$$

$P_{\vec{k}}$ is given by $T_{(\vec{k})i}(Z_c)$. Equation (11) shows that the effect of a motion purely parallel to the surface is just a displacement of the Fermi sphere by $\vec{Q}$. With suitable parameters eq. (11) may give a reduction in n_a with increasing $\vec{v}_{\parallel}$ such as seen experimentally in figure 1.

Unfortunately, eq. (9) is only soluble numerically [5] except for the wide band limit, that means for $\Delta(\omega)$ energy independent on the energy scale of Δ and $(E_F - E_a)$. Then the ω integral in eq. (8) defines a delta function and we have

$$i\dot{c}_a = [E_a(t) - i\,\tfrac{1}{2}\Delta(t)]\ c_a + \sum_{\vec{k}} T_{(\vec{k})i}(t) \times \exp\,[-i(E_{\vec{k}}t - E_{\vec{k}+\vec{Q}}t_o)]c^{o}_{\vec{k}+\vec{Q}} \tag{13}$$

where

$$\Delta(t) = |u(t)|^2\Delta \tag{14}$$

Integration of eq. (13) from $t \to -\infty$ to $t \to \infty$ and substitution of $c_a(\infty)$ into eq. (7) gives

$$\langle n_a(\infty)\rangle = \int\int_{-\infty}^{\infty} \sum_{\vec{k}} f(E_{\vec{k}+\vec{Q}}, E_F, T)\, |P_{\vec{k}}|^2\, u(t)u(t')$$

$$\times\, g(|\vec{k}|,t)\; g^*(|\vec{k}|,t')\,dtdt' \qquad (15)$$

where

$$g(|\vec{k}|,t) = \exp\{-i\,E_{\vec{k}}t - \int_{t}^{\infty} i\,E_a(t') + \tfrac{1}{2}\Delta(t')]dt'\} \qquad (16)$$

In eq. (15) we have assumed that the memory of the initial charge is lost. Again in eq. (15), the only effect of the parallel velocity is seen to be to displace the Fermi sphere.

Equation (15) can be converted to

$$\langle n_a(\infty)\rangle = \sum_{|\vec{k}|} \left| \int_{-\infty}^{\infty} \sqrt{\frac{\langle f(E_{\vec{k}+\vec{Q}}, E_F, T)\,|P_{\vec{k}}|^2\rangle_\epsilon}{\langle |P_{\vec{k}}|^2\rangle_\epsilon}}\cdot \tfrac{1}{2}\Delta(t)\; g(|\vec{k}|,t)dt \right|^2 \qquad (17)$$

where $\langle\ \rangle_\epsilon$ implies averaging over the surface $E_{\vec{k}} = \epsilon$ in $\vec{k}$ space.

First we will focuss on two analytical soluble situations.

For a motion parallel to the surface at a distance z_c eq. (17) can be converted into

$$\langle n_a(z_c)\rangle = \int_{-V_o}^{\infty} d\epsilon\, \frac{\langle f(E_{\vec{k}+\vec{Q}}, E_F, T)\,|P_{\vec{k}}|^2\rangle_\epsilon}{\langle |P_{\vec{k}}|^2\rangle_\epsilon}\cdot \frac{1}{\pi}\, \frac{\tfrac{1}{2}\,\Delta(z_c)}{(\epsilon - E_a(z_c))^2 + \dfrac{\Delta(z_c)^2}{4}} \qquad (18)$$

Here is $-V_o$ the position of the bottom of the conduction band with respect to the vacuum level. We see here that the main contribution to $\langle n_a(z_c)\rangle$ coming from $\vec{k}$ states wherefore $|E_{\vec{k}} - E_a| < \tfrac{1}{2}\,\Delta$.

Another analytical soluble situation is E_a = constant, $\Delta = \Delta_o \exp(-az)$ with $z = v_\perp t$ (uniform normal velocity). Then

$$\langle n_a(\infty)\rangle = \frac{1}{2av_\perp} \int_{-V_o}^{\infty} \frac{d\epsilon}{\cosh[\pi(\epsilon - E_a)/2av_\perp]}\, \frac{\langle f(E_{\vec{k}+\vec{Q}}, E_F, T)\,|P_{\vec{k}}|^2\rangle_\epsilon}{\langle |P_{\vec{k}}|^2\rangle_\epsilon} \qquad (19)$$

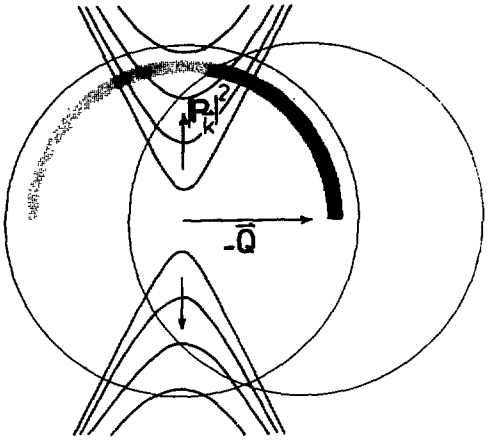

Fig. 2 - Sketch of the contours of $|P_{\vec{k}}|^2$ and the Fermi spheres $f(E_{\vec{k}}, E_F, T) = 1/2$ and $f(E_{\vec{k}+\vec{Q}}, E_F, T) = 1/2$. Vertical arrows show the direction of increasing $|P_{\vec{k}}|^2$. The dotted (half)ring indicates the resonant and filled states in case the Fermi sphere is not shifted. The dark ring section indicates the resonant and filled states in case the Fermi sphere is shifted over $\vec{Q}$.

The first term of the integrant is a peaked distribution with a width $av_\perp$, which is equal to the level width at the effective charge transfer distance z^* (freezing distance) as defined in [3,6] and chapter II. So also for this situation the contributions to $\langle n_a(\infty)\rangle$ are coming from $\vec{k}$ states wherefore $|E_{\vec{k}} - E_a| < \frac{1}{2}\Delta(z^*)$.

The characteristic decrease of $\langle n_a(\infty)\rangle$ with increase of $\vec{v}_\parallel$ (whereas it increases with $v_\perp$) seen in figure 1, comes from the decreased number of metal states which are resonant and filled (the dark area in figure 2) and from the anisotropy of $|P_{\vec{k}}|^2$ (see figure 2). Approximately $|P_{\vec{k}}|^2 \approx \exp(-b\, k_\parallel^2 + (b-a)\, k_\perp^2)$, where the H^- orbital is approximated by $\exp(-r^2/2b)$, and $a = 2z^*/\sqrt{\Phi}$, where Φ is the work function, and z^* is the effective

charge transfer distance. In figure 2 we see now that the resonant and filled states are situated in a region where $|P_{\vec{k}}|^2$ is small. Calculations with the simple formula (19) confirm that the effect is of the right order of magnitude.

In fact the affinity level of hydrogen will vary quite strongly with Z, as is known from Local Density Functional Calculations [7], lying below E_F at small Z but at large Z approaching 0.75 eV below vacuum, which lies above E_F. Starting from eq. (17) and by assuming that the main contributions to $<n_a(\infty)>$ are coming from $\vec{k}$ states around $E_{\vec{k}} \approx E_a(Z)$ and that they are on the scale of $\Delta(Z)$ not strongly dependent on ϵ, we can approximate eq. (17) by

$$<n_a(\infty)> \approx \int_{-V_o}^{\infty} dt \left| \int_{-\infty}^{\infty} \sqrt{N^-(Z(t))\ \tfrac{1}{2}\Delta(t)} \right.$$

$$\left. \exp\{-i\epsilon t - \int_t^{\infty} [i\ E_a(t') + \tfrac{1}{2}\Delta(t')]\ dt'\} dt \right|^2 \qquad (20)$$

Herein $N^-(Z)$ is defined by $<n_a(Z)>$ of eq. (18).

The numerical calculations are performed by using eq. (20) and the model of chapter II to estimate $P_{\vec{k}} \approx T_{\vec{k}i}(Z)$ and $E_a(Z)$. The numerical calculations show good agreement with the experimental data (see figure 1).

3. CONCLUSIONS

In conclusion we have described the effect of the parallel velocity $\vec{v}_{||}$ on the spinless Anderson model theory of resonant charge exchange where for jellium surfaces it acts to displace the Fermi sphere by $\vec{Q} = \vec{v}_{||}$. The comparison with the experimental data for H^+ on cesium covered tungsten is satisfactory.

REFERENCES

[1] A. Blandin, A. Nourtier and D. Hone, J.Physique 37 (1976) 369; A. Nourtier, These d'Etat, Orsay (1976).

[2] W. Bloss and D. Hone, Surface Sci. 72 (1978) 277.

[3] R. Brako and D.M. Newns, Surface Sci. 108 (1981) 253.

[4] R. Brako and D.M. Newns, Vacuum 32 (1982) 1.

[5] K.L. Sebastian, V.C. Jyothi Bhasu and T.B. Grimley, Surface Sci. 110 (1981) L571.

[6] E.G. Overbosch, B. Rasser, A.D. Tenner and J. Los, Surface Sci. 92 (1980) 310.

[7] H. Hjelmberg, O. Gunnarsson and B.I. Lundqvist, Surface Sci. 92 (1980) 310.

CHAPTER V

The Scattering of Hydrogen from Cesiated Tungsten Surfaces

ABSTRACT

The reflection of protons from a partially cesiated tungsten surface is studied in the energy domain between 100 and 2000 eV and in the angular domain between 75° and 85° with respect to the surface normal. The study is performed by measuring the angular and energy distribution of the scattered negative ions.

The reflection can take place along two pathes. One path is reflection from the cesium surface layer, the other one is reflection from the tungsten substrate. A dependence of the final charge state on the path is observed. It is inferred that this phenomenon is due to incomplete neutralization of the protons scattered from the cesium layer.

The energy loss of the reflected ions cannot be accounted for by using only the binary collision model. Also the electronic stopping of the atoms by the metal electrons is shown to be an important energy loss mechanism.

Total conversion measurements of H^+ to H^- combined with the measurements of the negatively charged fraction of the scattered particles, as reported in chapter III, yield the particle reflection coefficient as a function of the angle of incidence. These reflection coefficients show that for angles of incidence less than 75° already more than 50% of the particles do not reflect from the surface.

Total conversion efficiency measurements with H^- ions as primary ions show that the influence of the initial charge state on the total conversion is very small.

1. INTRODUCTION

In chapter III the negatively charged fraction of hydrogen scattered from a cesiated tungsten surface is studied. The dependence of this charged fraction on the normal as well as the parallel velocity component could be determined. This efficient H^- formation process can be applied in low energy neutral hydrogen detectors and in the large H^- sources required for nuclear fusion (100 A and 200 keV). For these applications it is, however, also important to know which fraction of the particles reflects from the surface and how large the energy loss of these particles during the reflection is.

Until recently most attention, theoretical as well as experimental, was paid to the reflection process of normal incident hydrogen atoms and molecules [1,2,3,4]. The interest is mainly coming from the importance of normal incidence in plasma wall interactions. For the above mentioned applications of the surface H^- formation process it is, however, preferable to use grazing angles of incidence. For grazing angles the reflection coefficient will increase and the energy loss will decrease. The hydrogen reflection process for grazing angles and low energies (< 2000 eV) has been subject of just a few numerical studies [5], especially for the combination of grazing angles and covered surfaces a very limited amount of data, experimental as well as theoretical, is available. In this paper we will now discuss the reflection of grazing incident protons from cesiated tungsten, the incident energy is below 2000 eV. We will limit ourselves to protons as incident ions, the reflection of molecular hydrogen ions will be discussed in a next paper. In section 2 the apparatus by which the measurements are performed is described and in section 3 the results are discussed.

2. THE APPARATUS

The apparatus in principle can be separated into two chambers, the primary beam line chamber and the UHV vacuum chamber (see figure 1). In the primary beam line chamber an H^+, H_2^+ or H_3^+ beam in energy ranging from 20 eV to 10000 eV, with an opening

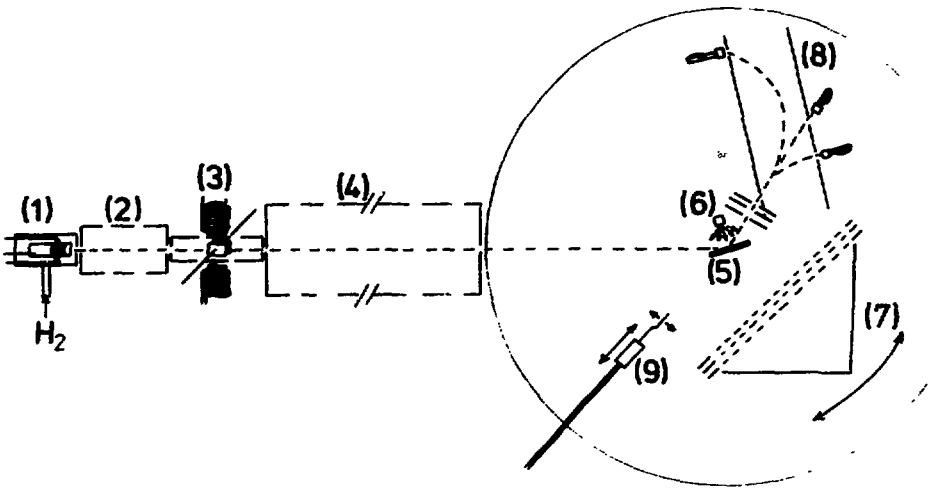

Fig. 1 - Schematic view of the experimental set up: (1) is the ion source, (2) the stripper, (3) the Wien filter, (4) the Heddle lens system, (5) the target, (6) the cesium dispenser, (7) the Faraday cup, (8) the energy analyser, (9) the Kelvin probe.

angle of approximately 0.5^{o} (FWHM) and a beam diameter of 1 mm can be made. In the UHV chamber the target and the detector are placed. In the following we will first describe the primary beam line.

The beam line consists of an ion source, a stripper, a mass selector and a five-cylinder acceleration and deceleration lens system.

2.1. The ion source:

The ion source is an electron impact source (see [1], in figure 1). The acceleration voltage of the electrons is roughly 40 V. The hydrogen pressure in the source is of the order of $1.0\ \ 10^{-2}$ Torr. The ions which can be extracted from the source are H^{+}, H_2^{+}, H_3^{+} and, if the extraction voltage is reversed, also H^{-}. The extraction voltage is 400 V.

2.2. The stripper:

After extraction collimation takes place. From the source an ion beam is extracted with a relative large angular spread. The stripper (see [2], in figure 1) now collimates this beam in such a way that all the particles in the beam leaving the stripper can fulfil the target (image) plane requirements with respect to opening angle and beam width of the final beam. Furthermore, the collimation is such that the intensity is maximum at the target. The requirements for a 400 eV beam are, 1 mm diameter and 0.5^{o} opening angle in the image plane. The stripper is a three-cylinder lens system which is operated in the einzellens mode. The focal points are located in the entrance and exit planes of the lens; so that width and opening angle of the beam can be chosen independent of each other by chosing the diameters of exit diaphragm and entrance diaphragms, respectively. The stripper is placed in a differentially pumped chamber. The pressure is $1.0\ \ 10^{-5}$ Torr.

2.3. The Wien filter:

In the Wien filter the ions are selected on mass (see [3], in figure 1). A Wien filter consists of a magnetic and an elec-

tric field perpendicular to each other. Both fields are perpendicular to the beam propagation direction. For one specific velocity the magnetic force is compensated by the electrostatic force and so only one specific mass will go straight on. Ions with different masses are deflected out of the beam. The velocity for which the filter is transparent is given by

$$v = \frac{|\vec{E}|}{|\vec{B}|}$$

The mass resolution is determined by the absolute value of magnetic and electric field strength. To increase the mass resolution without increasing the fields to unpracticle high values, the filter is placed in the middle element of a lens system consisting out of three rectangular tubes with heights much larger than their widths. Therefore focusing occurs in only one plane; the plane perpendicular to the focusing plane of the Wien filter. The complete configuration of Wien filter and lens therefore has focusing in two dimensions. The lens system is operated as an einzellens with a decelerating central lens element. Therefore the particles have a relatively small velocity, in the middle tube where the Wien filter is located. Consequently with relatively low electric and magnetic fiels a good resolution can be achieved.

2.4. The Heddle lens system:

In the Heddle lens system (see [4], in figure 1) the particles can be accelerated up to 10 keV or decelerated down to 20 eV. In principle this lens system consists out of two three-cylinder lens systems. In our case these are separated by a long cylinder which acts on the same hand as the last cylinder of the first lens system and as the first cylinder of the last lens system. The lens system is used in the Heddle mode [6] which means that the focal point of the first lens coincides with the focal point of the second one. The advantage of this operation mode is that a beam coming in with a zero beam angle also leaves the system with a zero beam angle. In the lens itself the beam stays also rather close to the axis so that lens

aberations do not play an important role. The angular and image magnification are both equal to the $1/4^{th}$ power of the acceleration or deceleration factor. This means that the magnification does not vary much with energy. The differentially pumped chamber of the lens system has a pressure of $1.0\ 10^{-7}$ Torr.

2.5. The UHV chamber:

The beam line chamber and the UHV chamber are separated by a pumping resistance. The working pressure in UHV chamber is $1.0\ 10^{-9}$ Torr which is obtained by a turbo-molecular pump and a titanium sublimation pump.

2.6. The target:

The target (see [5], in figure 1) is mounted in the center of the UHV chamber. It can rotate about the central axis of the chamber; the front of the target coincides with the central axis. The target is the (110) surface of a single crystal tungsten ribbon, the dimensions of the crystal are 15 by 2 by 0.2 mm. The crystal is supported by two tungsten rods. By ohmically heating it can be heated up to 2700 K. For the cleaning of the crystal a standard oxygen treatment [7] is used. The cleaning procedure is checked by LEED and Auger measurements. The cesium deposited on the surface comes from a cesium dispenser. The dispensers are obtained from SAES Getters, Italy. The dispenser is mounted 10 mm in front of the tungsten crystal.

The work function of the target is measured with a vibrating capacitor (Kelvin probe) method which is calibrated by the photo-electric method. Most measurements are performed with a cesium coverage of half a monolayer which corresponds to a work function of 1.45 eV and with a thick cesium layer which corresponds to a work function of 2.15 eV. At room temperature the thick cesium layer corresponds to a coverage of one monolayer [8]; a thicker layer will evaporate until one monolayer is established. The work function of a thick cesium layer is 2.15 eV.

2.7. The total conversion measurements:

To do total conversion measurements, it is necessary to measure the positive current hitting the target and the negative current reflected from the target. The positive current is measured as follows: Above the target, on the same support as the target, a diaphragm is mounted with an opening with exactly the same dimensions and position as the target crystal. The support can be shifted downwards until the diaphragm is in beamline. With a Faraday cup (see [7], in figure 1) which is positioned behind the diaphragm the total current which hit the target can thus be measured absolutely. The reflected negative particles are measured with the same large Faraday cup so that all the reflected ions can be measured. The measurements are performed with low work function surfaces. This implies that, with respect to the surrounding high work function material (≈ 4 eV), there is a potential difference. Because of this potential, a part of the positive beam is deflected from the surface. In the diaphragm measurements of the primary beam this effect is not present and so the total conversion efficiency will be underestimated. To compensate for this contact potential difference the target is kept on a potential of respectively -2.5 and -1.8 V depending on whether a partial cesium layer or a thick cesium layer is used.

2.8. The Faraday cup:

The Faraday cup (see [7], in figure 1) can rotate about the central axis of the system. The opening angle of the cup in the plane containing the beam line and the surface normal is 60°, the total opening angle is 1/4 π sterad. In front of the cup three grids are placed. Starting from the cup, the first grid is to retard the secundary electrons created by the particles which hit the inner walls of the cup. The voltage on that grid is -30 V. The second grid is to retard those positive ions of the primary beam which flow around the target and hit the Faraday cup directly. The voltage of this grid is 10 Volts more than the energy of the primary beam. The last grid is on ground potential and shields the chamber from the electric fields in the cup.

2.9. The energy analyser:

Differential measurements can be performed by replacing the Faraday cup by a parallel plate energy analyser (see [8], in figure 1). The plates are positioned under 45^{o} with respect to the incoming particles. The distance between entrance and exit slit is 100 mm, the width of both slits is 1.3 mm. In front of the analyser a three-slit lens system is placed, with this lens the acceptance angle of the analyser can be varied between 1^{o} and 6^{o}. This gives rise to a change of the intensity of the energy spectrum as well as to a change of the energy resolution. So the energy resolution can be varied between 0.5% and 4%. Furthermore, it is possible to operate the analyser system in a decelerating mode. The particles are then decelerated in the lens system before they enter the analyser. For the retarded particles the relative energy resolution stays the same but, because of the decreased nominal particle energy, the absolute resolution decreases.

Above 400 eV the charged fraction of the scattered particles can be determined. When no voltages are applied to the analyser the total amount of particles which goes straight through the analyser will be detected by a channeltron. When voltages are applied only the neutral particles impinge on the channeltron. By using the channeltron detection efficiencies for H and H^{-} of Crandall et al. [9] the charged fraction as function of the scattering angle can be determined. The relative intensity of the scattered positive and negative currents can be determined by comparing the absolute intensities of the energy spectra of the scattered H^{+} and H^{-} ions.

3. RESULTS AND DISCUSSION

In chapter III the velocity dependence of the negatively charged fraction of the scattered hydrogen atoms was considered. It turned out that the normal as well as the parallel velocity component were influencing the final charge state. In this chapter we will mainly concentrate on the scattering process. This will be done by discussing the measured angular

and the energy distributions of the scattered particles and the reflection coefficients deduced from the measurements.

3.1. The scattering distribution

In figure 2 the angular distribution of hydrogen atoms scattered from a partially cesium covered surface is shown. The primary beam energy is 400 eV and the angle of incidence is respectively 85°, 80° and 75° with respect to the surface

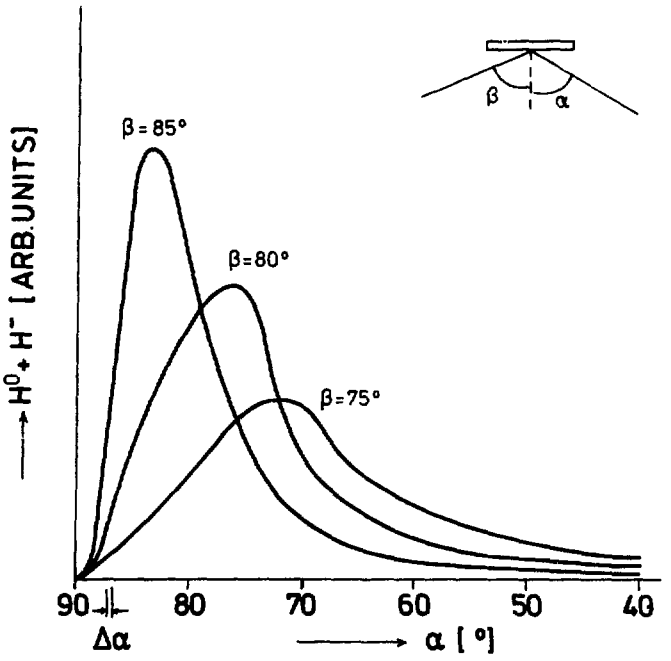

Fig. 2 - The angular distribution of the scattered particles ($H^0 + H^-$). The surface is a cesiated tungsten surface (Φ = 1.45 eV), the incident energy is 400 eV.

normal. The scattering distribution is more or less specular, with a FWHM of respectively 9.0°, 13.6° and 18.5°. The rather broad angular distributions lead to the idea that, despite the grazing angles of incidence and so despite of the low normal velocities, the surface is not flat. Penetration of the surface therefore will play an important role in the scattering process.

In figure 3 the energy distributions of the scattered H^- particles are shown. The parameters are the angles of incidence and detection. The energy of the primary particles is 1000 eV. Most curves show a double peak structure, corresponding to energy losses of the order of 5% and 15%. For decreasing angles of incidence or detection these peaks shift to higher energies. The large energy loss of up to 20% cannot be explained by a binary collision model. The binary collision model gives rise to energy losses of the order of 0.5%.

These observations lead to the following conclusions. The hydrogen atoms apparently are scattered from the surface along two pathes. The first path is reflection from the cesium surface layer, the second one is reflection from the tungsten substrate layer. The tungsten surface is the (110) plane, so the grazing incident atoms can be caught in a surface half channel. For 1000 eV hydrogen on tungsten the acceptance angle for channeling is of the order of 20^o. So despite the fact that the exact orientation of the crystal is not known we may assume that the probability for being caught in a surface half channel is large. Because the crystal is fixed in the chamber, this supposition cannot be checked by rotating the crystal around the surface normal. In the surface channels the electron density is rather high and so the amount of stopping by the metal electrons is considerable, the stopping by the tungsten nuclei will be of minor importance. The stopping power for 1000 eV hydrogen atoms in tungsten is of the order of 1.5 eV/a_o [10]. This means that on the average the particles stay for 80 a_o in a surface channel, hereafter scattering out of the surface channel will take place.

We will now apply this qualitative model to the date in figure 3. More grazing angles in general give rise to a longer path along the surface and will have a larger energy loss. This behaviour is seen in figure 3 where for a fixed angle of incidence the energy loss increases with increasing scattering angle. For a fixed scattering angle α and different angles of incidence β, see e.g. $\alpha = 80^o$ and $\beta = 85^o$, 80^o and 75^o, however, the energy loss is almost the same. Probably the path length in a surface channel is not strongly dependent on the incident angle.

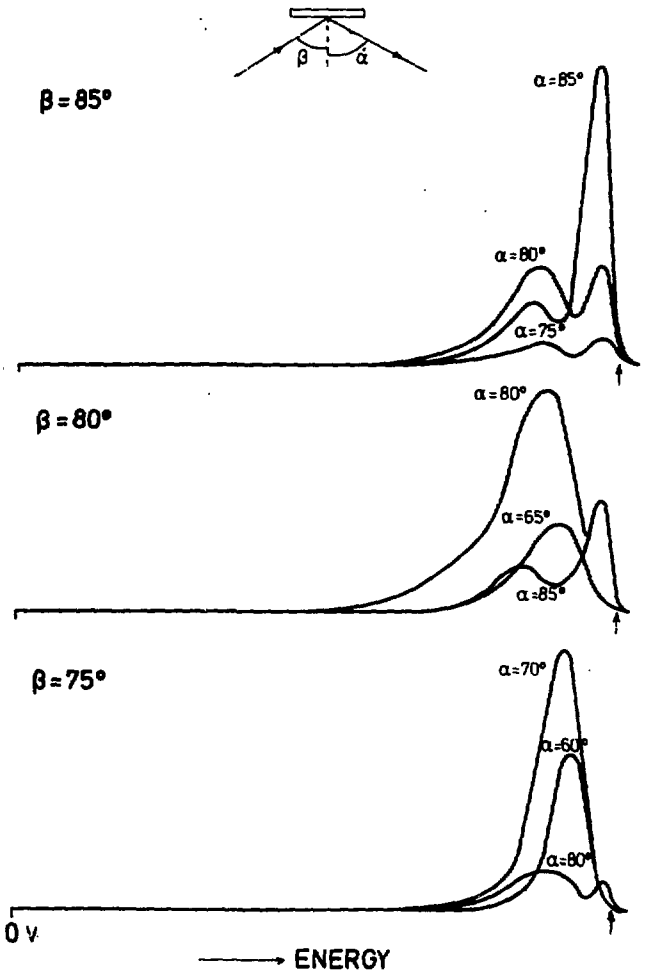

Fig. 3 - The energy distribution of the scattered H^- ions. The surface is a cesiated tungsten surface ($\Phi = 1.45$ eV), the incident energy is 1000 eV. The angle of incidence is 85^o, 80^o and 75^o, respectively. The primary energy is indicated with an arrow.

The evidence that the peak with the large energy loss is coming from tungsten scattering is also coming from the fact that for a clean tungsten surface this peak, which now has a very low intensity, is at the same position. The peak which we contributed to scattering from the cesium surface layer is absent.

As to be expected the number of ions reflected from cesium is strongly dependent on the angle of incidence. Increasing angles of incidence show an increasing amount of particles reflected from the cesium layer. Also the particles reflected from the cesium layer have an energy loss (3%) which is much larger than the energy loss expected from the binary collision model (0.5%). Probably also in the cesium layer the particles will undergo multiple collisions. Because the position of cesium atoms on the tungsten crystal is less ordered than the tungsten crystal itself [11] the path along the surface will be shorter. This combined with a stopping power of cesium which is a factor of 4 smaller than that of tungsten, the energy loss will be much lower.

3.2. The dependence of the final charge state on the reflection path

In figure 4 the negatively charged fraction is measured as a function of the scattering angle at the angles of incidence 85^{o} and 75^{o}. The primary energy of the incident protons is 400 eV. The charged fraction is 40% for angles of incidence of 75^{o} and 80^{o} and 35% for angles of incidence of 85^{o}. For 85^{o} angle of incidence much more particles scatter from the cesium layer than in the case of 75^{o} and 80^{o}. So probably the H^{-} formation probability is dependent on the fact whether the particles scatter from the cesium atoms or not. This behaviour is also measured by Eckstein et al. [2]; for normal incident hydrogen molecular ions on cesiated nickel they measure a lower H^{-} yield for particles scattered from the cesium atoms than for particles scattered from the tungsten substrate layer. The explanation of these results can be found in the incomplete neutralization of the incident protons.

The non-resonant neutralization process of the protons is strongly dependent on the metal electron density at the turning point of the trajectory of the scattered particles. As shown by Wojciechowski and by Rasser et al. [12,13] the ratio of the electron density at the tungsten surface and at the ce-

sium surface is of the order of 100. So for ions reflecting from the tungsten surface the neutralization probability is much larger than the neutralization probability for particles reflecting from the cesium surface layer.

After scattering the protons which were immediately neutralized in the ground state can become H^- in the outgoing trajectory. The protons, however, which did not neutralize or were neutralized in an excited state, can only become negative if the protons are first neutralized in the ground state. Because this neutralization or deexcitation process will take some time, the H^- formation process will start at relatively large distances from the surface. The final negative fraction thus will be smaller than in the case of a ground state atom leaving the surface.

Figure 4 shows that for low normal outgoing velocities the negatively charged fraction is independent of the angle of in-

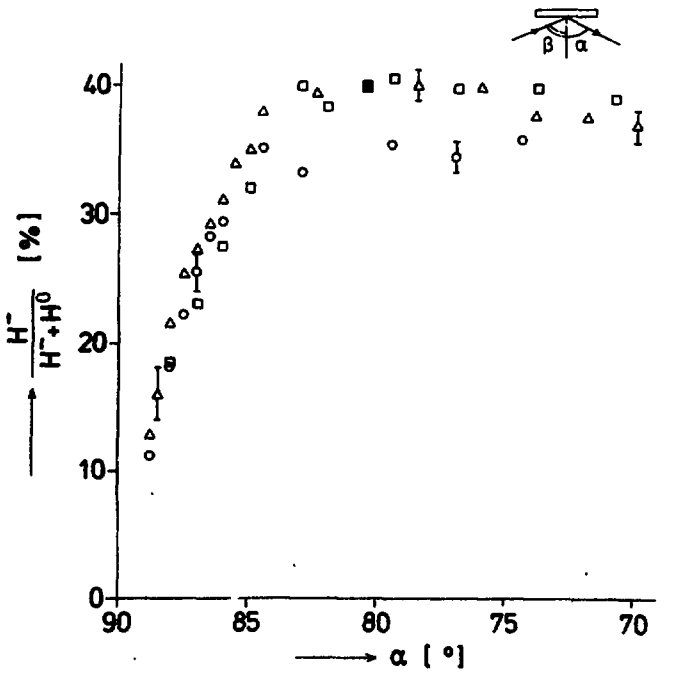

Fig. 4 -

The negatively charged fraction of the scattered particles as function of the scattering angle. The incident energy is 400 eV, the surface is cesiated tungsten (Φ = 1.45 eV). The angle of incidence is respectively 85° (o), 80° (Δ) and 75° (□).

cidence. For these velocities the neutralization probability in front of the surface is probably unity and it does not matter whether the particles scatter from cesium or tungsten. For scattering angles smaller than 75^{o} the data for angles of incidence of 75^{o}, 80^{o} and 85^{o} converge. From figure 3 can be seen that for these angles almost all the particles scatter from the tungsten surface, independent of the incident angle. So for decreasing angles the negatively charged fraction will converge to the same value. For normal incidence and large velocities (> 3.0 10^{5} m/s) Eckstein et al. [2] measured that more than 5% of the reflected particles is not neutralized at all, the survival probability is even larger for protons scattered from cesium. For these large normal velocities the neutralization is very insuffifient. It thus gives rise to a strongly reduced H^{-} yield compared to the yield obtained with particles starting as neutral at the surface.

3.3. The total H^{-} conversion efficiency

Figure 5 shows the total H^{-} conversion efficiency, that is the total reflected H^{-} current divided by the H^{+} current impinging on the target, as a function of the number of cesium depositions on the surface. A cesium deposition is obtained by heating the dispenser for a well-defined time. One deposition roughly corresponds to an increase of the cesium coverage with 0.35 10^{14} at/cm^{2}. In the figure also the work function is shown. The work function is measured after each cesium deposition. The energy of the incident protons is 400 eV and the angle of incidence is 82^{o}. From clean tungsten almost no H^{-} ions reflect from the surface. For increasing coverage the work function decreases while simultaneously the H^{-} yield increases. For an extensive discussion of the dependence of the H^{-} yield on the work function we refer to the preceding chapters.

Figure 6a and 6b show the total conversion efficiency as a function of the angle of incidence and energy of the primary protons. The surface is covered with half a monolayer cesium (Φ = 1.45 eV) and a thick cesium layer (Φ = 2.15 eV), respecti-

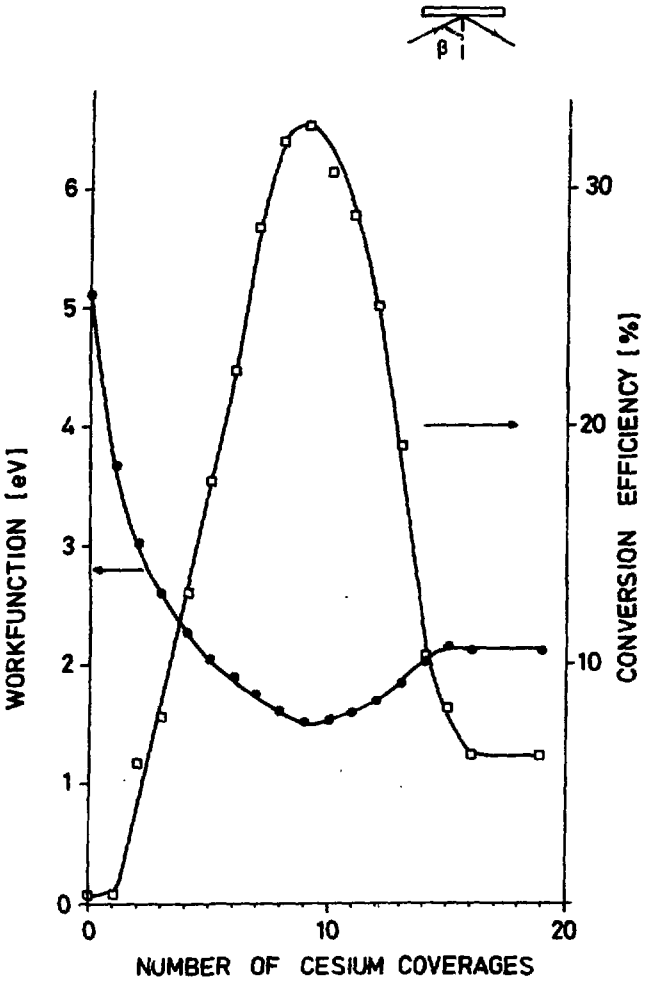

Fig. 5 -

The work function of the metal and the total H^- conversion efficiency as a function of the number of cesium coverages. A cesium coverage corresponds roughly to 0.35 10^{14} at/cm^2. The angle of incidence is 82^o. The energy of the H^+ ions is 400 eV.

vely. We first concentrate on reflection from a partly cesium covered surface. The maximum of the curves show a decrease with increasing total energy; this behaviour is also seen in the differential measurements, reported in chapter III and can be contributed to the finite velocity of the metal electrons. The decrease of the total conversion for large angles of incidence is due to the decreasing normal velocity of the scattered particles. This gives rise, according to figure 4, to a de-

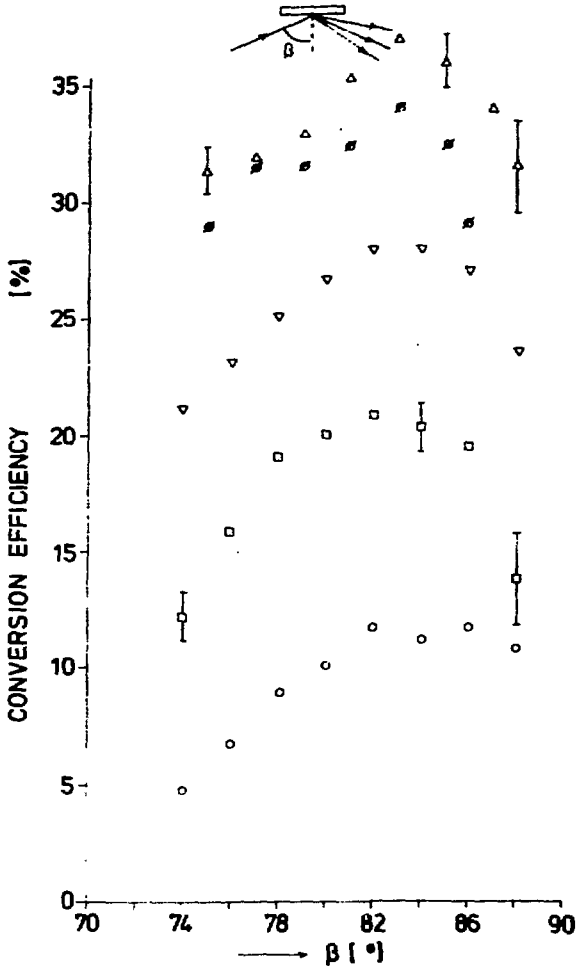

Fig.6a -

The total conversion efficiency as a function of the angle of incidence β. The data points are indicated by (ϕ) for 100 eV, by (Δ) for 200 eV, by (∇) for 400 eV, by (□) for 1000 eV and by (o) for 2000 eV. The work function of the surface is 1.45 eV.

creasing final H^- fraction. For decreasing angles of incidence the total conversion measurements show a decrease of the charged fraction. The explanation of this decrease can be found in a decrease of the reflection coefficient for these angles of incidence. The total conversion of scattering from a thick cesium layer (figure 6b) is much lower than in the case the surface is partially covered with cesium. For low energies (100 eV, 200 eV) increasing angles of incidence give decreasing con-

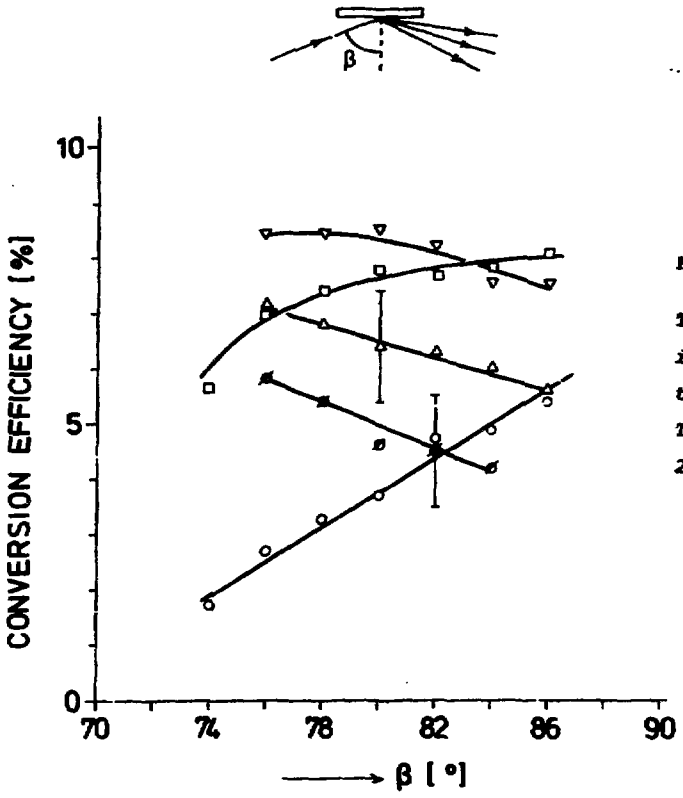

Fig. 6b-

The tungsten surface is here covered with a thick cesium layer. The work function is 2.15 eV.

version efficiencies. This can be understood in terms of a decreasing normal velocity which will give rise to a decreasing H^- fraction. For larger energies (2000 eV) the conversion increases for increasing angles. This can be understood in terms of an increasing reflection coefficient dominating the decrease of the conversion because of decreasing normal velocity.

3.4. The reflection coefficients

From the charged fraction measurements of the scattered particles as reported in chapter III and the total conversion measurements as reported in this chapter we can make an estimate of the reflection coefficients. To this end we make use of the following assumptions: (1) the particles reflect specularly from the surface; (2) no broadening of the scattering distributions takes place; (3) the energy loss during the reflection will be neglected; and (4) the charged fraction of the scattered particle is only dependent on the outgoing velocity. The results of this estimate are shown in figure 7.

Figure 7a shows the reflection coefficient for scattering from a tungsten surface covered with a thick cesium layer and figure 7b the reflection coefficient for scattering of a par-

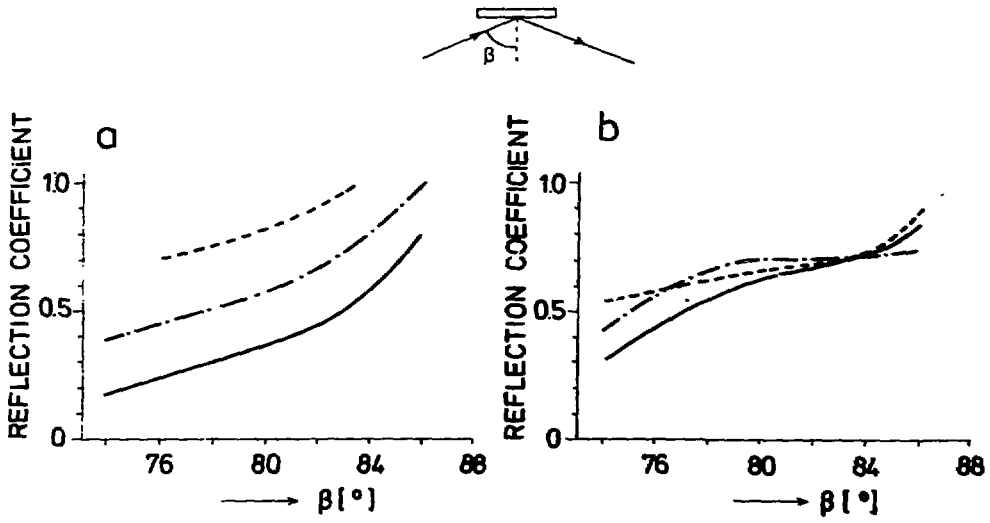

Fig. 7a - The reflection coefficient as function of the angle of incidence. The incident energy is respectively 400 eV (-----), 1000 eV (-.-.-) and 2000 eV (———). The measurements are performed at a thick cesium layer.

Fig. 7b - The tungsten surface is here partially covered with cesium. The work function is 1.45 eV.

tially cesiated tungsten surface. The angular regime is from 74^{o} to 86^{o}. As expected we see that the reflection coefficient increases for increasing angles. The most striking of these results is, that at an angle of 74^{o} the reflection coefficient for 1000 eV and 2000 eV is of the order of 30%, which is very low. It comes close to the reflection of hydrogen from graphite as reported by Eckstein et al. [3]. The influence of the density of the cesium layer on the reflection coefficient clearly can be seen for 400 eV. Here the reflection coefficient is significantly higher for a thick cesium layer than for a partial cesium layer.

3.5. H^- ions as primary particles

The influence of the initial charge state on the charge state after scattering is studied by scattering H^- instead of H^+ from the surface. The total "conversion" efficiency, is now defined as the H^- current reflected from the surface divided by the primary H^- current hitting the surface. Within the experimental accuracy, the dependence of the conversion efficiency on the cesium coverage is the same for H^- and H^+ ions (figure 5). So for clean tungsten almost all the H^- ions reflect as H^o while for increasing cesium coverage the H^- yield increases and is again maximal for minimum work function. In figure 8 the total conversion efficiency is shown as a function of the primary energy and the angle of incidence. The cesium coverage is such that the work function of the surface is minimal ($\Phi = 1.45$ eV). Also the total conversion measurements with H^+ as primary ion of figure 6a are shown. This figure shows that within the experimental accuracy there is no difference between both sets of measurements. From the measurements in figure 5 and 8 one can conclude that H^- ions reflecting from a clean tunsten surface, or in case of a cesium coverage from the tungsten under layer, will be neutral at the surface. In the outgoing trajectory the atoms can again pick up an electron, this depending on the work function.

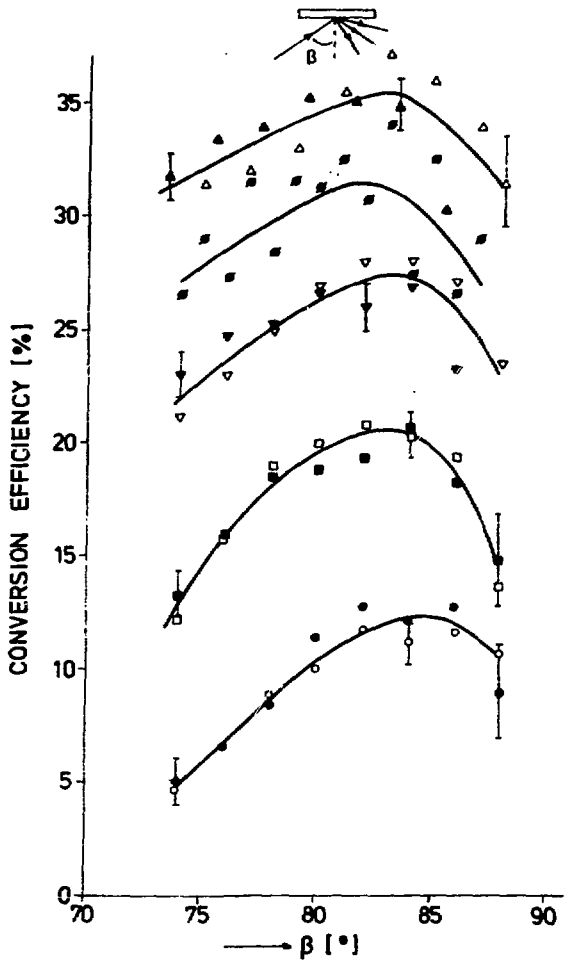

Fig. 8 -

The total conversion efficiency as a function of the angle of incidence β. The open data points are measurements with H^+ as primary ion; the filled points are measurements with H^- as primary ion. The data points are indicated by (ϕ) for 100 eV, by (Δ) for 200 eV, by (∇) for 400 eV, by (□) for 1000 eV and by (o) for 2000 eV. The work function is 1.45 eV.

For ions reflecting from the cesium atoms one can expect a final charge state which depends on the charge of the initial ion. The H^+ ions can be converted at the cesium atoms to H^o or will stay H^+, the H^- ions will be converted to H^o. Conversion of H^- or H^o to H^+ is very improbable. As discussed at figure 4, the primary H^- ions can thus give rise, for angles of reflection smaller than 85°, to a larger H^- yield than H^+ ions. Within the experimental accuracy the measurements of figure 8 do not show this difference. Probably the fraction of particles reflected from the cesium atoms is too small to give a measurable effect in the total conversion efficiency.

4. SUMMARY AND CONCLUSIONS

In the energy and angular range considered we can summarize the reflection process of protons from a cesiated surface as follows: The protons can scatter along two pathes, one is scattering from the cesium surface, the other one is scattering from the tungsten substrate surface. If they scatter from the tungsten surface the particles have a large probability to be caught in a surface channel. They then move through a surface channel over a distance of approximately 80 a_o. In the channel the atom will loose energy due to collisions with metal electrons and, for a smaller amount, by collisions with the tungsten atoms. This gives rise to energy losses of the order of 15%. A part of the particles will finally scatter out of the surface channels. In the channels we expect that in the energy range under consideration almost all the ions are neutralized. After the neutral atoms have left the surface they can become H^-; the H^- formation probability is strongly dependent on the parallel as well as the normal velocity components.

The protons which scatter directly from the cesium layer have a small probability to reflect as proton; these protons have a smaller probability to become H^-. The reflection coefficient in the angular regime from 75^o to 85^o goes from 40% to 80%. These reflection coefficients for cesiated tunsten and grazing angles of incidence do not agree with the calculations by the computer codes MARLOWE and TRIM [3] for the reflection of hydrogen from materials as Cu and Au, but roughly agree with the calculations of the reflection of hydrogen on C.
The total H^- conversion efficiency can have values up to 35%. This large total efficiency makes the surface process applicable in low energy neutral hydrogen detectors and in large H^- sources to be used in future nuclear fusion experiments.
The dependence of the total conversion efficiency on the initial charge is negligible. So in a neutral hydrogen detector based on the surface process, H^+, H^o and H^- can be detected with the same efficiency.

References

[1] P.J. Schneider, K.H. Berkner, W.G. Graham, R.V. Pyle and J.W. Stearns, Phys.Rev.B23 (1981) 941.

[2] W. Eckstein and H. Verbeek and R.S. Bhattacharya, Surface Sci. 99 (1980) 356.

[3] W. Eckstein, H. Verbeek, Max-Planck Institut für Plasmaphysik, report IPP 9/32 (1979).

[4] S. Yamaguchi, K. Ozawa, Y. Nakai and Y. Sugizaki, Tokai Research Establishment, report JAERI-M 82-118 (1982).

[5] O.S. Oen and M.T. Robinson, Nuclear Instruments and Methods 132 (1976) 647.

[6] D.W.O. Heddle, J.Phys.E: Sci.Instr. 4a (1971) 981.

[7] J.A. Becker, E.J. Becker and R.G. Brandes, J.Appl.Phys. 32 (1960) 411.

[8] Chen-Show Wang, J.Appl.Phys. 48 (1977) 1477.

[9] D.H. Crandall, J.A. Ray and C. Cisneros, Rev.Sci.Instrum. 46 (1975) 562.

[10] H.H. Andersen and J.F. Ziegler, Stopping Powers and Ranges in All Elements, Vol. 3, Pergamon Press (1977).

[11] A.G. Fedorus and A.G. Naumovets, Surface Sci. 21 (1970) 426.

[12] K.F. Wojciechowski, Surface Sci. 55 (1976) 246.

[13] B. Rasser, J.N.M. van Wunnik and J. Los, Surface Sci. 118 (1982) 697; this thesis chapter II.

Summary

In this thesis electron transfer between atoms and metal surfaces in general is discussed and the negative ionization of hydrogen by scattering protons at a cesiated crystalline tungsten (110) surface in particular. Experimental results and a novel theoretical analysis are presented.

In chapter I a theoretical overview of resonant electron transitions between atoms and metals is given.

In the first part of chapter II atom-metal electron transitions at a fixed atom-metal distance are described on the basis of a model developed by Gadzuk. This Gadzuk model only describes the electron transitions between an atomic ionization level and a metal conduction band. On the basis of this model positive surface ionization of the alkalis is described consistently. To describe also negative surface ionization, the Gadzuk model is extended in this work to the electron transitions between an affinity level and a metal conduction band.

In the second part of chapter II the influence of the motion of the atom on the atomic charge state is incorporated. This is done with a probability method and with an amplitude method. In both methods the electron transitions are treated quantum mechanically and the nuclear motion classically. In the probability method the time evolution of the probability of being in a specific charge state is considered, in the amplitude method the time evolution of the corresponding wave function amplitude. A comparison between both methods is made.

Measurements presented in chapter III show a strong dependence of the fraction of negatively charged H atoms scattered at cesiated tungsten, on the normal as well as the parallel velocity component. In the above mentioned probability and amplitude mehtods only the normal velocity is a parameter. In chapter III we propose a mechanism, based on the finite velocity of the metal electrons, which takes into account the effect of the parallel velocity on the charge state. This mechanism is incorporated in the probability method. Model calculations show a satisfactory agreement between the experimental data and the theoretical method.

In chapter IV the proposed mechanism for the parallel velocity effect is incorporated in the amplitude method. Also with this method the agreement between experiment and theory is satisfactory.

The scattering process of protons incident under grazing angles on a cesium covered surface is studied in chapter V. This is done by measuring the angular and energy distribution of the scattered atoms and the reflection coefficients. From these data several possible trajectories of the nuclei at the surface can be concluded. The dependence of the charge state on the trajectory of the nucleus is studied. Furthermore it is shown that the charge state after scattering is independent of the charge state of the incident atoms.

Samenvatting

Dit proefschrift handelt over de overdracht van electronen tussen atomen en metaal oppervlakken. Er wordt hierbij voornamelijk ingegaan op de negatieve ionisatie van waterstof door verstrooiing van protonen aan een gecesieerd wolfraam (110) oppervlak. Zowel experimentele resultaten, als ook een nieuwe theoretische analyse worden gepresenteerd.

In hoofdstuk I wordt een theoretisch overzicht van resonante overdracht van elektronen tussen atomen en metalen gegeven. Zeer belangrijk voor het onderhavige werk is de theorie van Gadzuk.

Gadzuk ontwikkelde een model dat resonante overdracht van elektronen tussen een atomair ionisatieniveau en een metaal-geleidingsband beschrijft; de atoom-metaal afstand is hierbij vast. Met behulp van dit model is een consistente beschrijving van positieve ionisatie van alkali's aan metaaloppervlakken gegeven.

In het eerste deel van hoofdstuk II wordt het Gadzuk model uitgebreid met de overdracht van elektronen tussen een affiniteitsniveau en een metaal-geleidingsband. Een beschrijving van negatieve ionisatie wordt dan mogelijk.

In het tweede deel van hoofdstuk II wordt de invloed van de beweging van het atoom op de atomaire ladingstoestand nagegaan. Dit wordt gedaan met een waarschijnlijkheidsmethode en een amplitudemethode. Bij beide methoden wordt de beweging van de elektronen quantummechanisch behandeld en de beweging van de kern klassiek. Bij de waarschijnlijkheidsmethode wordt de tijdsevolutie van de waarschijnlijkheid om in een bepaalde toestand te verkeren beschouwd, bij de amplitudemethode de tijdsevolutie van de amplitude van de corresponderende golffunktie. Beide methoden worden met elkaar vergeleken.

De metingen in hoofdstuk III laten voor de ladingsfraktie na verstrooiing een sterke afhankelijkheid zien van de loodrechte en de parallelle snelheidscomponent. In de hierboven aangehaalde methode wordt alleen de normale snelheidscomponent in rekening gebracht. In hoofdstuk III wordt een mechanisme voor-

gesteld dat het parallelle snelheidseffekt kan verklaren. Aan dit mechanisme ligt de eindige snelheid van de elektronen in het metaal ten grondslag. Het mechanisme is in dit hoofdstuk volgens de waarschijnlijkheidsmethode verwerkt. Modelberekeningen laten een goede overeenstemming tussen experiment en theorie zien.

In hoofdstuk IV wordt het voorgestelde mechanisme in de amplitudemethode ingebouwd. Ook hier is de overeenstemming tussen theorie en experiment bevredigend.

Het verstrooiingsproces van scherend invallende protonen aan gecesieerde oppervlakken wordt besproken in hoofdstuk V. Dit wordt gedaan aan de hand van de hoekverdelingen en de energieverdelingen van de verstrooide atomen en van de reflectie coefficiënten. Uit deze gegevens blijkt dat er twee essentiëel verschillende banen aan het oppervlak mogelijk zijn. Er wordt nader ingegaan op de afhankelijkheid van de omladingswaarschijnlijkheid voor de verschillende deeltjesbanen. Verder blijkt de ladingstoestand na verstrooiing onafhankelijk te zijn van de ladingstoestand van het invallende waterstofatoom.

Nawoord

Mijn eerste kennismaking met het FOM-Instituut voor Atoom- en Molecuulfysica dateert van 1974; ik was HTS-stagiaire bij de BIOM groep. De dynamische sfeer die er heerste gecombineerd met de didactisch, uiterst analytische en toch menselijke benadering van mijn mentor, Piet Kistemaker, deed me mijn laatste twijfels over het gaan volgen van een universitaire studie overwinnen.

Na mijn kandidaatsexamen keerde ik terug op het Instituut. Mijn doctoraalstage en promotiewerk voerde ik uit onder de bezielende leiding van Professor Joop Los. Zijn grote kwaliteiten als wetenschapper en promotor en zijn menselijke gedrag, eenvoud en vriendelijkheid heb ik steeds zeer bewonderd en me als voorbeeld gesteld. Dankzij de stimulerende invloed van Joop heeft dit proefschrift zijn definitieve vorm gekregen.

Velen hebben hiernaast een bijdrage geleverd aan het totstand komen van dit proefschrift. Hen wil ik hier danken.

Professor J. Kistemaker wil ik danken voor de gelegenheid die hij geboden heeft, me onbekommerd in zijn dynamisch Instituur te ontplooien.

Veel dank ben ik verschuldigd aan mijn direkte experimentele opvoeder, Aart Kleyn. Zijn vele wijze lessen en adviezen hebben mijn leven als experimentator en ook mijn leven daarbuiten zeer veraangenaamd. Grote bewondering heb ik voor zijn enthousiasme en zijn uiterst inspirerende aanwezigheid. In de ontwerp en bouwfase van de apparatuur heb ik veel steun van Ernst Granneman ondervonden. Zijn energie en zijn efficiënte pragmatische aanpak benijd ik. Hans Geerlings ben ik zeer erkentelijk voor het vele meetwerk en de in alle opzichten plezierige samenwerking.

De Franse inbreng in dit proefschrift is van Bernard Rasser, met genoegen denk ik terug aan het jaar dat hij op het FOM-Instituut werkte. Zijn inspanningen hebben mede bijgedragen tot hoofdstuk II, en bezorgden mij, betreffende het theoretisch begrip van het proces, een vliegende start. Dr. Newns dank ik voor de gastvrijheid waarmee hij mij in de zomer van 1982 in

een door stakingen lam gelegd London heeft weten te ontvangen. Deze uiterst vruchtbare weken hebben aanleiding gegeven tot het theoretische hoofdstuk IV.

Zeer veel dank ben ik verschuldigd aan mijn co-referent professor dr. P.F. de Châtel, zijn zorgvuldige en kritische begeleiding van het uiteindelijke schrijven van dit proefschrift is de leesbaarheid duidelijk ten goede gekomen.

Aan de contacten met de DENISErs Peter Massmann en Pieter-Jan van Bommel zal ik met veel plezier blijven terugdenken. Henk Hopman en de overige leden van de TN-III groep dank ik voor de adviezen, vele technische steun en de aangename wijze waarop zij mij in hun groep hebben opgenomen. Thijs Bolhuis ben ik erkentelijk voor de inspanningen die hij zich getroost heeft bij de bouw van het apparaat. Hans Terhorst wil ik danken voor het bouwen, ombouwen en repareren van de vele elektronische kasten.

Alle leden van de moleculaire bundelgroep toonden steeds een grote bereidheid me op alle mogelijke manieren te steunen waarvoor dank.

Het in dit proefschrift beschreven werk kon alleen tot stand komen door de bereidwillige steun van alle technische, administratieve en onderhoudsmedewerkers van het Instituut, ik ben hen allen daar zeer erkentelijk voor.

Het feitelijke tot stand komen van dit boekje is het werk van Tine van der Veer: typewerk, Hanna Smid: tekeningen, Frans Monterie: fotografie en Henk Sodenkamp: drukwerk; elk van hen heeft dit op haar of zijn eigen zeer plezierige wijze gedaan.

Alle leden van het Instituut hebben bijgedragen aan de zeer prettige sfeer die de afgelopen 6 jaar voor me hebben doen omvliegen. Speciaal wil ik hiervan noemen de leden van de lopersgroep, de leden van de "praat en wijn club", mijn twee uiterst kleurrijke kamergenoten Ulfert Klomp en Mirano Spalburg en mijn mede sportfanaat Jacques Kimman.

Verder ben ik mijn ouders zeer erkentelijk voor hun voortdurende belangstelling en steun, en voor de gezelligheid tijdens mijn vele Limburgse "weekend-vakanties".

S T E L L I N G E N

bij het proefschrift

ELECTRON TRANSFER IN GAS SURFACE COLLISIONS

door

J.N.M. van Wunnik

Amsterdam, 19 januari 1983

1. De invloed van de parallelle snelheid $\vec{v}_{\parallel}$ op de ladingsfraktie van alkali atomen, welke verstrooid worden aan het oppervlak van een vrije elektronenmetaal is zeer groot. In de bestaande methoden voor de beschrijving van de loodrechte snelheidsafhankelijkheid kan de parallelle snelheidsafhankelijkheid verdisconteerd worden door in de $\vec{k}$ ruimte de bol van gevulde toestanden over een afstand $\hbar\vec{v}_{\parallel}$ te verschuiven.
   - *Dit proefschrift, hoofdstuk III en IV.*

2. De parallelle snelheidsafhankelijkheid van resonante ladingsuitwisselingsprocessen tussen een parallel aan een metaal oppervlak bewegend atoom en het metaal, biedt de mogelijkheid informatie te verkrijgen omtrent de parallelle snelheidsverdeling van metaalelektronen aan het oppervlak.

3. Bij de bestudering van de predissociatie van H_2 via triplet toestanden is het aan te raden deze toestanden te prepareren door H_2^+ aan cesium te neutraliseren.

4. Voor het optreden van dissociatie bij verstrooiing van moleculen aan metaaloppervlakken, is de uitwisseling van elektronen tussen de moleculen en het metaal een belangrijke faktor.
   - *W. Heiland en E. Taglauer; Nucl.Instr.Meth. 194 (1982) 667.*

5. Door gebruik te maken van zwelpoeder en het effect van demping door microbuiging, is het mogelijk op volledig optische wijze penetratie van vocht in glasvezelkabels te detekteren en te lokaliseren.
   - *J.T. Krause; Proc.Top.Meeting of Optical Fiber Communications, Washington DC (1979) 18.*

6. Er is experimenteel bewezen dat het mogelijk is elektronen ringen met stromen van 1 kA te versnellen. Indien zulke ringen kunnen worden versneld tot 10 MeV, zou men de beschikking krijgen over een zeer intense submillimeter stralingsbron.
   - *D. Taggart, M. Parker, H.J. Hopman and H.H. Fleischman; Twenty-fourth Annual Meeting Division of Plasma Physics (1982).*

7. Bij het gebruik van microkanaalplaten in plaatsgevoelige deeltjesdetektoren, waarbij men naast de plaats tevens geinteresseerd is in de grootte van de deeltjesflux, wordt het konditioneren van de platen ten onrechte vaak achterwege gelaten.
   - *D. Rees, J.Phys.E, Sci.Instr., 13 (1980) 763.*

8. Voor ionenbundels met ronde doorsneden kan de transmissie van een Wien filter verhoogd worden en de praktische uitvoering vereenvoudigd, door het filter op te stellen in de vertragende sectie van een einzellens systeem. De focusserende werking van de einzellens dient loodrecht op de intrinsiek focusserende werking van het filter te staan.
   - *W.H.J. Andersen, Brit.J.Appl.Phys. 18 (1967) 1573.*

9. Onder de kondities die Reiser aanneemt in zijn zgn. "smooth approximation" kan de ruimteladingsbegrensde stroom in periodiek focusserende quadrupool-kanalen, anders dan in de door hem gegeven benadering, ook analytisch exact berekend worden.
   - *Reiser; Part.Acc. 8 (1978) 167.*
   - *Reiser: J.Appl.Phys. 52 (1981) 555.*
   - *P.W. van Amersfoort, E.H.A. Granneman, J. Kistemaker, F. Siebenlist, R.W. Thomae, H. Klein en A. Schempp; FOM-report 55.120, appendix B (1982).*

10. Het belang van het bereiken van een nauwkeurige gedefinieerde eindtemperatuur in Curie-punt Pyrolyse Massa Spectrometrie van complex organisch materiaal wordt sterk overschat.
   - *H.L.C. Meuzelaar et al.; Anal.Chem. 45 (1973) 1546.*
   - *W. Windig et al.; J.Anal.Appl.Pyrol. 1 (1979) 39.*

11. Wat in de sport onder "afzien" wordt verstaan, is uitsluitend empirisch te begrijpen.